Ore Geology Reviews 39 (2011) 164–179

Contents lists available at ScienceDirect

Ore Geology Reviews

journal homepage: www.elsevier.com/locate/oregeorev

Age and primary architecture of the Copperton Zn-Cu VMS deposit, Northern Cape Province, South Africa

Russell Bailie [a,*], Jens Gutzmer [a,b]

[a] Paleoproterozoic Mineralisation Research Group, Department of Geology, University of Johannesburg, P.O. Box 524, Auckland Park, Johannesburg, 2006, South Africa
[b] Department of Mineralogy, TU Bergakademie Freiberg, Freiberg, Saxony, 09596, Germany

ARTICLE INFO

Article history:
Received 27 October 2009
Received in revised form 14 February 2011
Accepted 16 February 2011
Available online 24 February 2011

Keywords:
Copperton deposit
Areachap Group
Volcanogenic massive sulphide (VMS) deposit
Geochemistry
Geochronology

ABSTRACT

The Prieska Copper Mine (Copperton) deposit, located in the Northern Cape Province of South Africa, exploited from 1972 to 1994 a very large (ca. 47 Mt pre-mining resource) massive sulphide lens containing on average ca. 1% Cu and 2% Zn. The orebody occurred as a stratiform/stratabound tabular lens hosted by the subvertically dipping Copperton Formation, which is part of the intensely deformed and highly metamorphosed Areachap Group. The latter represents a 1.3-1.24 Ga continental volcanic island arc that was accreted onto the western margin of the Kaapvaal Craton during the initial stages of the 1.2-1.0 Ga Namaquan Orogeny. The present contribution is aimed at resolving important uncertainties surrounding the architecture, age and origin of this world class base metal deposit. Despite intense deformation and high-grade metamorphism the original architecture of the deposit is found to be unusually well preserved, with a stratabound zone of intense hydrothermal alteration below, and a series of characteristic cap rocks above the massive sulphide orebody. Geochemical data and radiometric ages for host rocks and massive sulphide ores lead to the conclusion that the Copperton deposit comprises a very large chimney-type volcanogenic massive sulphide deposit that formed at 1.28-1.29 Ga. The deposit meets many of the criteria of the bimodal-siliciclastic or bimodal-felsic types of VMS deposits.

1. Introduction

The Prieska Copper Mine (Copperton) deposit, situated along the eastern margin of the Proterozoic Namaqua Metamorphic Province of the Namaqua-Natal Belt, southern Africa, is one of the world's 30 largest VMS deposits (Galley et al., 2007). The deposit was discovered in 1968 and mined from 1972 to 1994. Wagener and Van Schalkwyk (1986) report a pre-mining resource of 47 Mt grading 1.7% Cu and 3.8% Zn to 900 m below surface. Galley et al. (2007) revised this to 47.2 Mt containing 0.98% Cu, 1.98% Zn and 20 g/t Ag after completion of mining. Relative to its size and economic importance the Copperton deposit has received relatively little attention in terms of scientific research, with only a few contributions in the published literature (Middleton, 1976; Theart et al., 1989; Uiterwyk and Frick, 1985; Wagener and Van Schalkwyk, 1986). The highly deformed and metamorphosed nature of the Copperton deposit has led to varied interpretations of its architecture and origin. Theart et al. (1989) identified the Copperton deposit as a highly metamorphosed example of a volcanogenic massive sulphide (VMS) deposit, but without placing any detailed constraints on its architecture and possible correspondence to less metamorphosed VMS deposits (e.g., Franklin et al., 2005; Galley et al., 2007). This short contribution reviews previously published geochemical and isotopic information and supplements existing geochronological data to provide a more concise understanding of the origin of this world-class Zn-Cu deposit.

2. Regional geological setting

The Copperton deposit occurs at the southern tip of the SE-NW striking exposure belt of the poly-deformed and highly metamorphosed Mesoproterozoic Areachap Group on the eastern margin of the Namaqua Metamorphic Province at its contact with the Archean Kaapvaal Craton (Fig. 1).

The Areachap Group is a prominent volcanosedimentary succession comprised of varying proportions of amphibolite, hornblende gneiss, biotite gneiss, quartzofeldspathic gneiss, calc-silicate and pelitic schists (Bailie et al., 2010a; Geringer et al., 1986, 1994), which has been interpreted as the remnant of a tholeiitic to calc-alkaline volcanic island arc (Bailie et al., 2010a; Barton and Burger, 1983; Geringer et al., 1986, 1994; Thomas et al., 1994) that formed at ca. 1.3-1.24 Ga along the margin of the Kaapvaal Craton in response to eastward directed subduction (Bailie et al., 2010a). This arc was accreted onto the western margin of the Kaapvaal Craton early during the ~1.2-1.0 Ga Namaquan Orogeny, during which it was extensively

* Corresponding author at: Department of Earth Sciences, University of the Western Cape, Private Bag X17, Belville, Cape Town, 7535, South Africa. Tel.: +27 21 959 2637; fax: +27 21 959 1317.
E-mail addresses: rbailie@uwc.ac.za (R. Bailie), jens.gutzmer@mineral.tu-freiberg.de (J. Gutzmer).

0169-1368/$ – see front matter © 2011 Elsevier B.V. All rights reserved.
doi:10.1016/j.oregeorev.2011.02.001

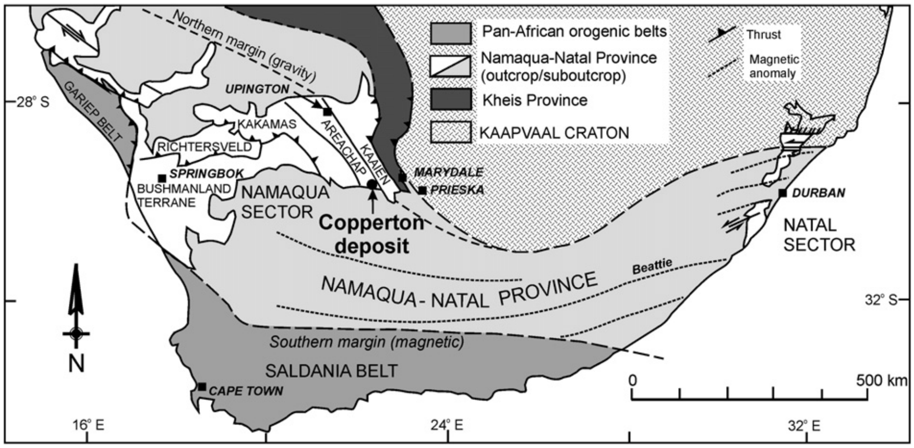

Fig. 1. Simplified geological map of southern Africa showing the location of the Copperton deposit on the eastern margin of the Namaqua Sector of the Namaqua-Natal Province at its contact with the Archean Kaapvaal Craton (modified after Cornell et al., 2006).

metamorphosed and deformed (Geringer et al., 1986; Pettersson et al., 2007). Along its ~280 km long known strike extent, the Areachap Group is host to a number of stratiform/stratabound Zn-Cu massive sulphide deposits (Fig. 2). Of these, the Copperton deposit is by far the largest and the only one that has been fully exploited.

The Copperton deposit is hosted by the Copperton Formation comprised of the Smouspan Gneiss, Prieska Copper Mines Assemblage (PCMA) and the Vogelstruisbult Member (Geringer et al., 1994; Fig. 3). Metamorphism of the Copperton Formation reached upper amphibolite to lower granulite facies grade with a temperature estimate of 680-720 °C and a pressure estimate of 5.5 kbar by Cornell et al. (1990a, 1992). Three major deformational events are recognized (Humphreys et al., 1988; Theart, 1985) of which the first (D_1) gave rise to the main penetrative foliation and is now present as intrafolial folds (F_1). The

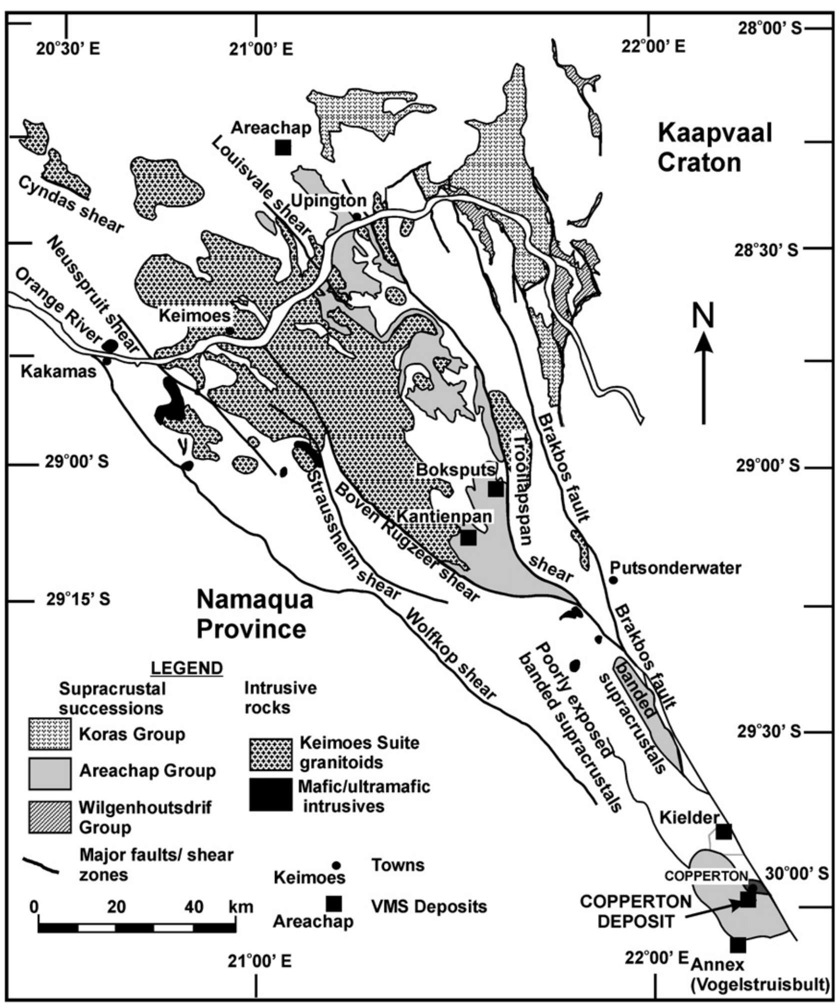

Fig. 2. Simplified geological map of the volcanosedimentary successions on the eastern margin of the Namaqua Province. The location of the Copperton deposit at the southern end of the Areachap Group, along with other volcanogenic massive sulphide deposits, is shown (modified after Geringer et al., 1988, 1994).

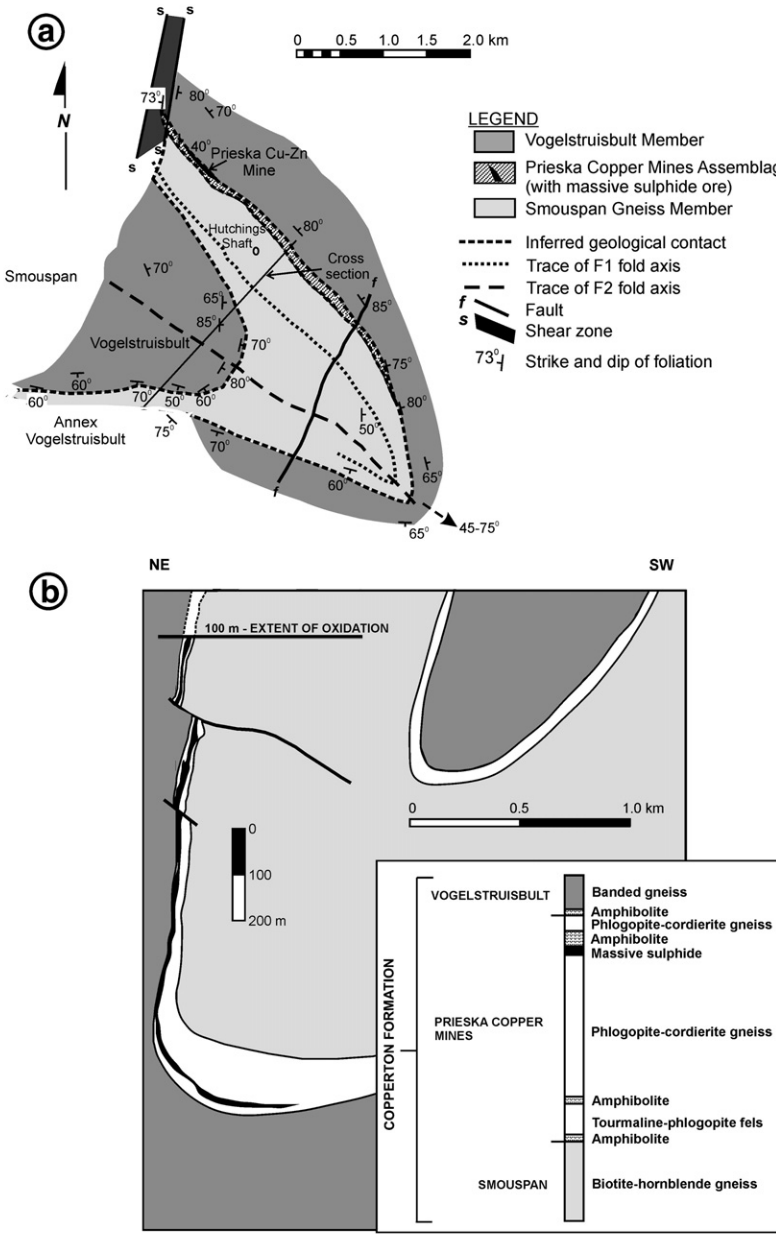

Fig. 3. a. Surface geology of the Copperton deposit (after Theart et al., 1989). b. Simplified geological cross-section of the Copperton deposit (modified after Theart, 1985 and Wagener and Van Schalkwyk, 1986).

subsequent deformational event (D_2) gave rise to tight NW-NNW-oriented F_2 folds with a steep easterly dip, with the later D_3 deformation giving rise to open NE-ENE-oriented F_3 folds. The latter deformation event is of only minor effect at the Copperton deposit (Humphreys et al., 1988). High grade metamorphism is associated with the earlier phases of deformation and the associated intrusion of syn- to post-tectonic granitoids of the Keimoes Suite (Cornell et al., 1992; Geringer et al., 1988). The later phases of deformation led to the development of shears and an associated retrograde metamorphic overprint (Theart, 1985).

The tabular massive sulphide ore-body strikes northwest-south-east and extends along strike for just over 2000 m. It persists to a depth of at least 1000 m, with a plunge of 45°, which at depth generally exceeds 60° (Fig. 3). The orebody is broadly concordant with the host rock succession, with an average width of 10 m (varying between 0.5 to 32 m - Uiterwyk and Frick, 1985). The bedding of the host rock generally dips between 60 and 85° to the northeast on the northern side of the orebody, and between 60 and 80° to the southwest on the western side of the orebody with a general NNW-NW strike (Fig. 3). The orebody occurs on the northeastern flank of a tight NW-SE striking and SE plunging asymmetric anticlinal synform (F_2 fold) developed in the Copperton Formation, with the geological footwall in the center of the fold (Fig. 3). Theart et al. (1989) suggested that the succession is overturned so that the structural hanging wall (Smouspan Gneiss) is the stratigraphic footwall to the massive sulphide orebody. The rocks at the Copperton deposit are bound to the east by the Copperton shear zone which is the most westerly exposure of the Brakbos Fault system in the southern end of the Areachap Belt. The Copperton deposit is separated from the Vogelstruisbult (Annex) deposit to the south by the Klipgatspan shear zone (Humphreys et al., 1988), a major splay of the Copperton shear zone (Scheepers, 1989).

The Copperton orebody has been oxidized and leached from the present-day land surface to a depth of 100 m (Fig. 3b). Composed of massively textured and hard iron oxides (limonite and goethite) with some secondary Cu minerals (minor malachite and azurite), the gossan of the Copperton deposit was noticeable but did not form prominent outcrops above the thin cover of Cenozoic windblown sand

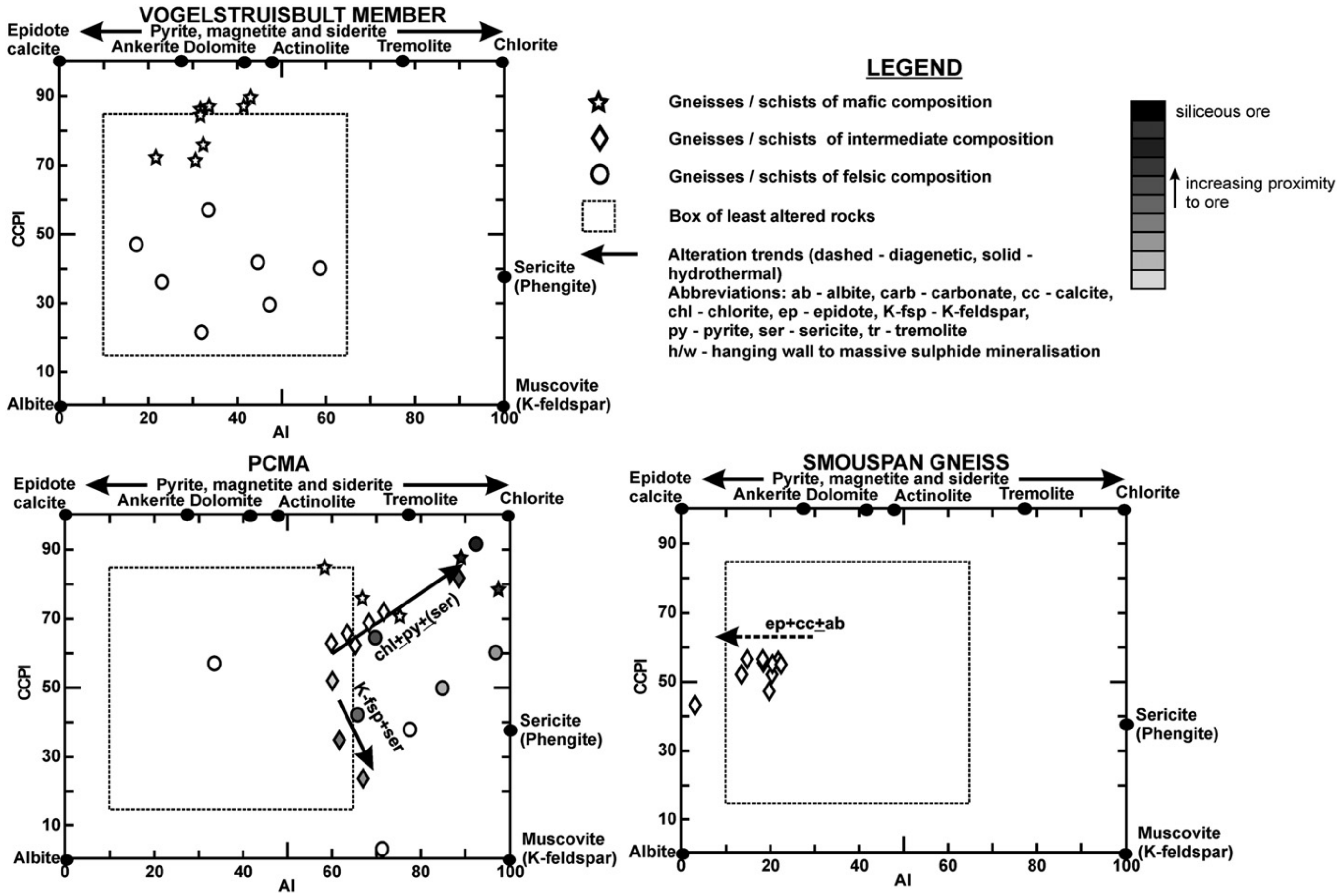

Fig. 4. Alteration box plot of Large et al. (2001) for the three members of the Copperton Formation at the Copperton deposit, with the boxes being the fields of unaltered volcanic or volcaniclastic rocks and the arrows representing various diagenetic and hydrothermal alteration trends that affect volcanic rocks (modified after Bailie et al., 2010a).

and calcrete. At depth, the oxidized material was found to be soft and porous, with good textural preservation of the pre-existing sulphide minerals (Middleton, 1976). The transition from gossanous material to unaltered massive sulphide has been described as sharp (Middleton, 1976).

3. Lithological architecture

Bailie et al. (2010a) studied 54 drill core samples from the Copperton deposit (Tables A1 to A4). This data formed part of a regional geochemical study of the Areachap Group with the geochemistry published by these authors interpreted on a regional scale rather than on a local scale. The mineralogy of the different lithotypes is listed in Table A1. The geochemical data (after Bailie et al., 2010a) are given in appendix tables with average major element data for the various lithologies given in Table A2, trace element data given in Table A3 and rare earth element (REE) data in Table A4. The geochemistry of the Copperton deposit is summarized in a series of geochemical plots, modified after Bailie et al. (2010a), that make use of immobile trace elements, given in Figs. A1 to A3. The Sm-Nd isotope characteristics of the deposit, taken from Bailie et al. (2010a), are given in Fig. A4 and Table A10. Analytical techniques and errors for major, minor and trace element and Sm-Nd isotopic analyses are reported with the relevant tables.

The following description of the detailed lithological architecture of the Copperton deposit progresses from footwall to hanging wall of the massive sulphide orebody, following Theart (1985) and Theart et al. (1989). Apart from the trace element geochemical classification and description of the lithologies given in Figs. A1 to A3, whole rock geochemical data for each of the three stratigraphic units of the Copperton Formation are illustrated in alteration box plots (Fig. 4). The alteration box plot of Large et al. (2001) relates whole-rock geochemistry to potential alteration minerals present in the samples and is constructed with two alteration indices, the Hashimoto alteration index [$AI = 100(MgO + K_2O)/(MgO + K_2O + CaO + Na_2O)$; Ishikawa et al., 1976], and a chlorite-carbonate-pyrite index [$CCPI = 100(FeO + MgO)/(FeO + MgO + Na_2O + K_2O)$]. Despite the use of the mobile alkali elements for the alteration indices, this plot has been shown to be of use for metamorphosed VMS deposits in high-grade terrains (Theart et al., in press).

The Smouspan Gneiss is a thick homogeneous calc-alkaline biotite-hornblende gneiss (Fig. 5a) of dacitic composition. The gneisses have Nb/Y ratios of 0.3 and Zr/TiO_2 ratios varying between 0.025 and 0.030 and are characterised by LREE-enrichment [$(La/Sm)_N = 2.04$-4.02; $(La/Yb)_N = 1.95$-7.62] and prominent negative Eu anomalies [$(Eu/Eu^*)_N = 0.21$-0.73]. They show strong depletions in Nb, Ta, Sr, Zr and Ti, and are enriched in Th, U and Pb when normalised to primitive mantle values and have predominantly subduction-related volcanic arc granite characteristics in the Nb-Y and Ta-Yb tectonic discrimination diagrams of Pearce et al. (1984) (Fig. A3).

The dacitic Smouspan Gneiss exhibits weak to moderate epidote ± calcite ± albite alteration (Fig. 4), which is a common diagenetic alteration trend in intermediate and mafic volcanic rocks (Large et al., 2001). The presence of this alteration in the stratigraphic footwall to the mineralisation rather than in the other lithological units (Fig. 4) suggests that is likely to be more of a localised pre-metamorphic rather than a pervasive post-metamorphic effect.

The Smouspan Gneiss is gradationally overlain by the lithologically complex PCMA (Theart et al., 1989). The PCMA forms a 10 to 100 m thick succession of mostly fine-grained and laminated gneisses

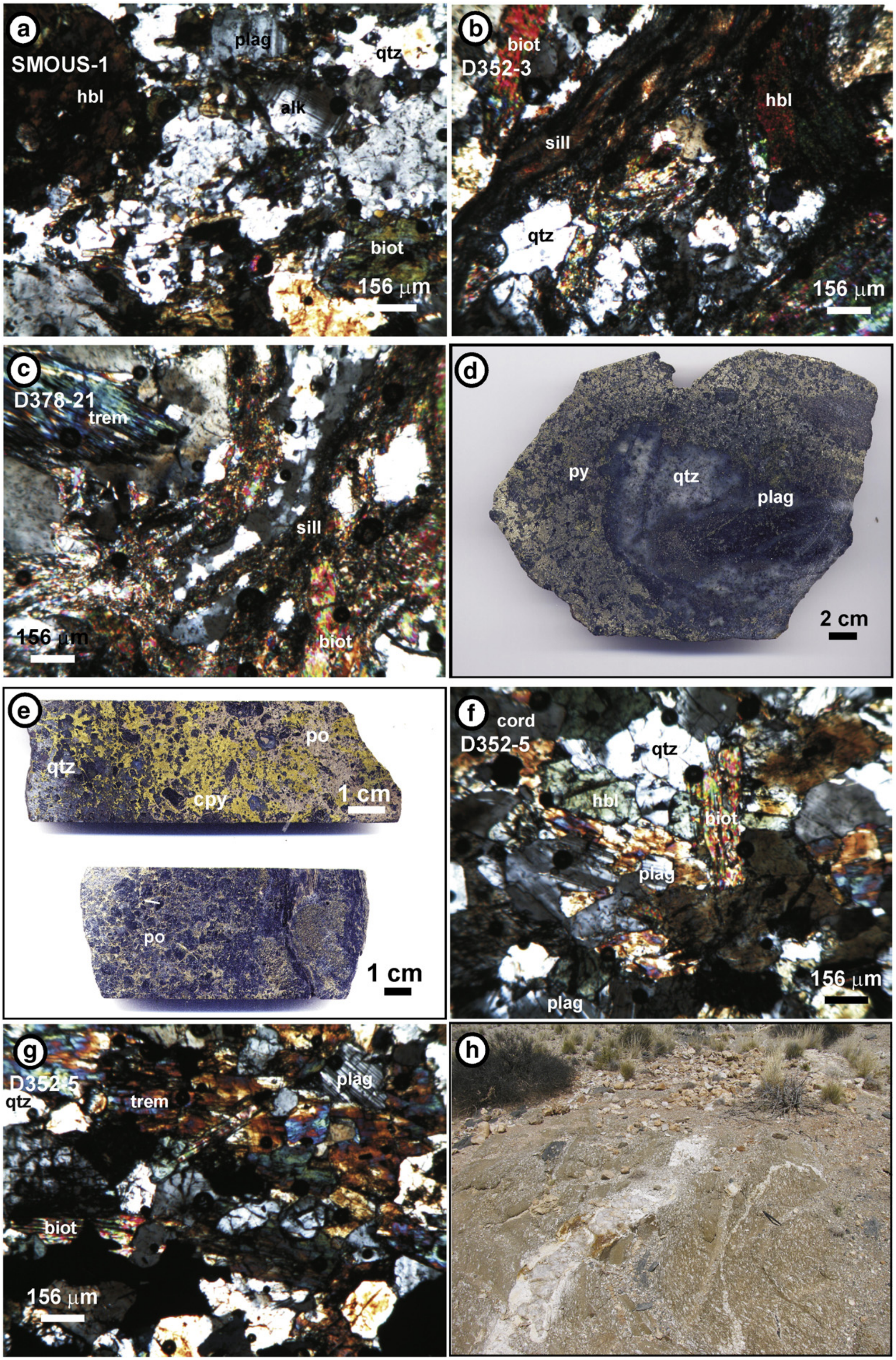

a
SMOUS-1
plag
qtz
hbl
alk
biot
156 μm
b
biot
D352-3
hbl
sill
qtz
156 μm
c
D378-21
trem
sill
156 μm
biot
d
py
qtz
plag
2 cm
e
qtz
po
cpy
1 cm
po
1 cm
f
cord
D352-5
qtz
hbl
biot
plag
plag
156 μm
g
D352-5
qtz
trem
plag
biot
156 μm
h

(Wagener and Van Schalkwyk, 1986; Fig. 5b, c) and is approximately 100 m thick below and 20 m thick above the massive sulphide lens (Theart et al., 1989) in the fully developed succession. The PCMA can be subdivided into three lithologically distinct units, including coarse-grained tourmaline-phlogopite-albite-gedrite and phlogopite-sillimanite-cordierite gneisses that immediately underlie the orebody (Theart et al., 1989), the massive sulphide orebody itself, and an immediately overlying, variable succession of pyrite-quartz, carbonate-anhydrite and manganese-rich magnetite lithologies (Wagener and Van Schalkwyk, 1986). In contrast to the weakly altered Smouspan Gneiss the footwall lithologies of the PCMA are characterised by intense alteration as denoted by the unusual lithologies.

The gneisses of the PCMA that comprise the footwall to the massive sulphide orebody (Fig. 4) predominantly represent Mg-enriched compositionally immature sedimentary/volcaniclastic or volcanic protoliths derived from an intermediate provenance, as denoted by their Ni concentrations and high Zr/TiO_2 ratios (Bailie, 2008). Immobile trace elements and trends in the alteration box plot (Fig. 4) readily identify the Smouspan Gneiss as the likely protolith. The alteration box plot further reveals that the transformation of the Smouspan Gneiss to the variable lithologies of the PCMA was prompted by hydrothermal chlorite + pyrite ± sericite alteration (Fig. 4). The altered lithologies were metamorphosed to phlogopite-cordierite-gedrite gneisses, in accordance with interpretations of previous authors (Schade et al., 1989; Theart, 1985; Theart et al., 1989).

Much of the Copperton orebody is comprised of massive sulphide containing more than 50% sulphide minerals (Middleton, 1976). Pyrite is always the predominant sulphide mineral, with variable amounts of chalcopyrite and sphalerite, accompanied locally by pyrrhotite, minor galena and magnetite, and trace amounts of marcasite, molybdenite, wehrlite, arsenopyrite and gudmuntite (Uiterwyk and Frick, 1985). The sulphides are typically fine- to medium-grained and associated with variable amounts of silicate (tremolite, phlogopite, tourmaline, diopside and pseudomorphs of serpentine after forsterite), sulphate (barite, anhydrite) and carbonate (calcite) gangue (Theart, 1985; Wagener and Van Schalkwyk, 1986). Barite occurred as a minor constituent throughout the orebody. Whilst its abundance co-varies with that of the sulphides, its distribution correlates inversely with that of chalcopyrite. Carbonate and calc-silicate minerals occur in greater abundance near the stratigraphic hanging wall, with sphalerite typically associated with carbonate and barite (Wagener and Van Schalkwyk, 1986).

Distinct textural and mineralogical subtypes of massive sulphide ore, as defined by Middleton (1976) and Uiterwyk and Frick (1985), are distinguished by the presence of centimeter-sized, usually crushed pyrite porphyroblasts ('porphyroblastic ore'), the abundance of sphalerite ('sphalerite-rich ore'), and the presence of rounded host rock fragments in the massive sulphide matrix ('hackly ore' by Middleton, 1976; 'durchbewegung texture' of Theart, 1985) (Fig. 5d, e). Whereas the sphalerite-rich ore occurred towards the fringes of the orebody, the durchbewegung-textured ore became abundant with depth (Wagener and Van Schalkwyk, 1986). In good agreement with the observed distribution of textural and mineralogical ore types the Copperton deposit appears broadly zoned with respect to its metal content, with Cu enriched along the central strike of the orebody and Zn and Pb concentrated along the outer fringes (Middleton, 1976; Wagener and Van Schalkwyk, 1986). Lead, though present only in minor concentrations, was found to be particularly abundant near the stratigraphic top of the orebody, and in the immediate hanging wall (Wagener and Van Schalkwyk, 1986). The base metal tenor of the deposit corresponds closely to many other VMS deposits associated with juvenile crust (Barrie and Hannington, 1999; Fig. 6).

Sulphur isotope data, recording $\delta^{34}S$ values for 34 sulphides and a single sulphate sample from the Copperton deposit yield $\delta^{34}S$ values for the sulphides varying between 4.9 and 7.4‰ (with a single anomalous value of −13.1‰) and a $\delta^{34}S$ value of 18.5‰ for a single barite sample (Bailie et al., 2010b; Theart, 1985). Based on these results magmatic sulphur with a variable contribution of thermochemically reduced marine sulphate can be identified as the primary sulphur source for the formation of Fe-Zn-Cu sulphides of the Copperton deposit, with contemporaneous seawater, which would have had a $\delta^{34}S$ value of ~17‰, regarded as the primary source of sulphate for barite formation (Bailie et al., 2010b).

The massive sulphide orebody is overlain by a thin and complex succession of unusual lithotypes that occur in close association with the massive sulphide orebody (Wagener and Van Schalkwyk, 1986). These lithologies include a finely laminated fine-grained pyritic quartzite commonly in sharp contact with the massive sulphide orebody, a carbonate-sulphate-rich lithology composed of dolomite, calcite, barite and serpentine, with millimeter-wide layers of anhydrite, as well as a manganese-rich magnetite zone comprised of magnetite, rhodonite, carbonates, barite, spessartine garnet, diopside and amphibole. All these lithologies occur as lensoid, laterally discontinuous bodies, with the pyritic quartzite extending beyond the limits of the massive sulphide orebody (Wagener and Van Schalkwyk, 1986).

The PCMA is overlain by an ~1000 m thick heterogeneous gneiss of a general banded appearance termed the Vogelstruisbult Member that is comprised of amphibolite, biotite gneiss, hornblende gneiss, hornblende biotite gneiss, diopside-bearing calc-silicate gneiss and sillimanite-garnet-biotite-cordierite gneiss (Uiterwyk and Frick,

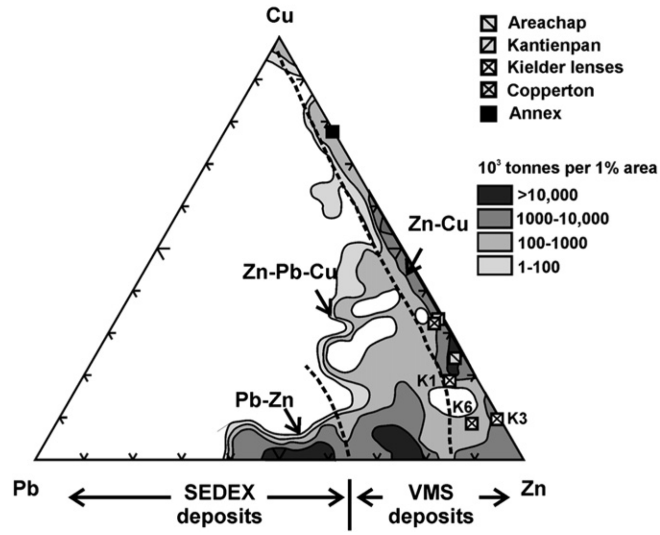

Fig. 6. Base metal content of the Areachap Group deposits. Pb-Zn-Cu ternary plot (after Franklin et al., 1981 and Franklin, 1993) indicating the predominant Zn-Cu nature of the Areachap Group deposits.

Fig. 5. Photos and photomicrographs of the rock types and textures of the Copperton massive sulphide deposit. a. Biotite-hornblende gneiss, Smouspan Gneiss Member, Copperton Formation, Copperton Mine, sample SMOUS-1. b. Amphibole gneiss, PCMA, Copperton Formation, Copperton Mine, sample D352-3. c. Biotite gneiss, PCMA, Copperton Formation, Copperton Mine, sample D378-21. d. Polished block from the Copperton Mine showing "durchbewegung" texture wherein rounded blocks of host rock occur within a pyritic groundmass. The pyrite has undergone brittle failure, having recrystallised and/or replaced silicate minerals in certain areas. e. Two core pieces from drill core D306 from the Copperton Mine, the first showing "durchbewegung" textures in which remobilized sulphides (chalcopyrite and pyrrhotite) contain small rounded "clasts" of quartz and other gangue minerals. The second core (lower photo) shows disseminated, remobilized pyrrhotite within a quartz phlogopite groundmass. Note the *rounded fragment* on the *right side* of the core section. f. Amphibole gneiss, Copperton Formation, Vogelstruisbult Member, Copperton Mine, sample D352-5. g. Amphibole gneiss, Vogelstruisbult Member, Copperton Formation, Copperton Mine, sample D352-5. h. Strongly foliated augen-textured amphibole gneiss crosscut by pegmatitic veining. Abbreviations: *alk* alkali feldspar, *biot* biotite, *cord* cordierite, *cpy* chalcopyrite, *hbl* hornblende, *plag* plagioclase, *po* pyrrhotite, *py* pyrite, *qtz* quartz, *sill* sillimanite, *trem* tremolite.

1985; Fig. 5f-h). These compositionally diverse gneisses and amphibolites were derived from both immature sedimentary / pyroclastic rocks of intermediate composition (Bailie, 2008) and a diverse range of volcanic rocks. The rocks of the Vogelstruisbult Member were subjected to minor diagenetic alteration, and possibly limited hydrothermal alteration as the gneisses of mafic composition fall immediately outside the least altered box, whereas those of felsic composition show a spread away from the expected area of felsic composition within the least altered box (Fig. 4).

Quantitatively minor amphibolites occur throughout the succession (see also Theart et al., 1989), but are especially concentrated in the Vogelstruisbult Member. Two types of amphibolite occur. The first type, which shows fine compositional lamination (Theart, 1985; Theart et al., 1989), is considered to represent high-Fe sub-alkaline tholeiitic lava flows (Figs. A1 and A2) forming part of the metasedimentary succession (Theart, 1985). The second type of amphibolite is typically coarse-grained and composed of hornblende and oligoclase. These occur throughout the Copperton Formation and are thought to be tholeiitic basaltic sills intruded into the succession prior to deformation and metamorphism (Theart, 1985; Theart et al., 1989).

4. Radiogenic isotopes and geochronology

The ortho-amphibolites forming part of the succession have $\varepsilon_{Nd(t)}$ values varying between +3.52 and +5.51 (Table A5), indicating derivation from a depleted mantle source (Bailie et al., 2010a; Cornell et al., 1986; Fig. A4). These values are similar to those for the metadacitic Smouspan Gneiss which has $\varepsilon_{Nd(t)}$ values of +1.96 to +3.30 (Table A5; Bailie et al., 2010a; Cornell et al., 1986), also denoting a mantle derivation but with a minor crustal component.

As VMS deposits are formed at, or near the seawater-rock interface and are preserved by an influx of sediment or renewed volcanism that terminates the hydrothermal mineralization event, a similarity in ages between the hanging wall and footwall lithologies can be expected (Franklin et al., 2005). Furthermore, since metals are usually leached from the immediately underlying rock pile (Verati et al., 1999), good agreement between Pb isotope values and model ages obtained from ore-forming sulphides and footwall rocks is usually observed (Franklin et al., 2005). These characteristics can thus be used as criteria to test the origin of putative VMS deposits in highly metamorphosed and deformed terranes where the original nature and architecture of the deposit have been obscured. For the Copperton deposit Pb isotope data and model ages were previously obtained by Cornell et al. (1990a), Köppel (1980) and Theart (1985) and Pb-Pb ages obtained on zircon were published by Cornell and Pettersson (2007) and Cornell et al. (1990b). All of these ages are in good agreement with one another and suggest that the Smouspan Gneiss and the formation of the Copperton massive sulphide orebody occurred between ~1280 and 1300 Ma (Table 1). Furthermore, Köppel (1980) noted that, based on the Pb isotope composition of four samples of galena from the Copperton deposit, the lead in the Copperton orebody shows characteristics of lead of mantle origin with no crustal influence.

Cornell et al. (1990b) obtained a Pb-Pb zircon age from the Smouspan Gneiss of the Copperton Formation and Cornell and Pettersson (2007) dated a garnet-biotite-two feldspar-quartz-cordierite metapelitic gneiss from the Vogelstruisbult Member, i.e., the hanging wall to the Copperton deposit (Table 1). This existing geochronological data set was complemented with precise U-Pb SHRIMP ages for zircons separated from a putative volcaniclastic unit of the Vogelstruisbult Member, along with a sample of the Smouspan Gneiss.

The Smouspan Gneiss sample (Smous-1) used for the extraction of zircons is a weakly-foliated biotite-hornblende-plagioclase gneiss (Fig. 5a). The sample selected from the Vogelstruisbult Member (COP06-8) is a strongly-foliated amphibole gneiss comprised of hornblende, quartz, biotite, alkali feldspar, fibrolitic sillimanite, garnet and magnetite, with alternating leucocratic and melanocratic bands. From its geochemical characteristics (low Zr, Hf, La and Ce contents, high Sr and V contents and low Zr/TiO_2 ratios (0.002)) it is a mafic volcaniclastic/metasedimentary rock having a sub-alkaline basalt composition. Similarly, the Smous-1 sample of the Smouspan Gneiss has similar low Zr, Hf, La and Ce contents and low Zr/TiO_2 ratios and also has a sub-alkaline basalt composition despite being a sample of the dacitic Smouspan Gneiss. The whole rock major and trace element geochemistry of both samples is given in Tables A6 to A8.

Zircons separated from the Smouspan Gneiss (Smous-1) are small, typically 100–150 μm, subhedral, with concentric zonation patterns that are typically disturbed or disrupted by dark, unzoned transgressive patches. Cornell et al. (1990b) described similar zircons that they dated from the Smouspan Gneiss. Many of the magmatic zircons from the Smouspan Gneiss are marked by extensive common lead giving rise to large error ellipses (Fig. 7a). Extensive Pb-loss has also caused a large and variable degree of discordancy (Fig. 7a; Table A9). On the U-Pb concordia plot the zircons define a chord with an upper intercept of 1283 ± 12 Ma and a lower intercept of 292 ± 30 Ma (MSWD = 1.06) (Fig. 7a). A mean $^{207}Pb/^{206}Pb$ age of 1268 ± 11 Ma (MSWD = 0.21, probability = 0.98) is within error of the intercept age as well as the age of 1285 ± 14 Ma obtained by Cornell et al. (1990b) from the same unit by single zircon thermal ionization mass spectrometry (TIMS). A single concordant zircon (analysis 14.1 – Table A9) has a $^{207}Pb/^{206}Pb$ age of 1277 ± 11 Ma. Two

Table 1
Radiometric age data available for the Copperton deposit listed from hanging wall (top) to footwall (bottom) (modified after Moen, 2007).

Geological Unit	Method	Age (Ma)	Event Dated	Reference
Vogel [a]	U-Pb (zircon - probe)	1286 ± 8	magmatism	this study
ore	Pb-Pb (sulphides)	1305 ± 100	ore formation	Köppel (1980)
ore	Pb-Pb (galena)	1300	ore formation	Middleton (1976)
ore	Pb-Pb (sulphides)	1288 (μ_2 = 9.975)	ore formation	Theart (1985)
ore	Pb-Pb (sulphides)	~1250	ore formation	Cornell et al. (1990a)
Smouspan	Sm-Nd (whole rock)	1514 ± 80	magmatism	Cornell et al. (1986)
Smouspan	Sm-Nd (whole rock)	1350 ± 138	magmatism	Cornell et al. (1986)
Smouspan	Pb-Pb (whole rock)	1323 +268/-294	magmatism	Theart (1985)
Smouspan	Rb-Sr (whole rock)	1312 ± 110	metamorphism	Cornell (1978)
Smouspan	U-Pb (zircon- TIMS[b])	1285 ± 13	magmatism	Cornell et al. (1990b)
Smouspan	U-Pb (zircon - probe)	1283 ± 12	magmatism	this study
Vogel	U-Pb (zircon - probe)	1282 ± 45	magmatism	Cornell and Pettersson (2007)
Smouspan	Pb-Pb (whole rock)	1268 ± 100	magmatism	Cornell et al. (1990b)
Smouspan	Rb-Sr (whole rock)	1210 ± 38	metamorphism	Cornell et al. (1986)
Smouspan	U-Pb (whole rock)	1165 ± 115	metamorphism	Theart (1985)
Smouspan	U-Pb (whole rock)	1097 ± 236	metamorphism	Theart (1985)
Smouspan	Ar-Ar (hornblende)	1080	cooling	Cornell et al. (1986)
Smouspan	Pb-Pb (whole rock)	1077 +176/-186	metamorphism	Theart (1985)

[a] Vogel – Vogelstruisbult Member.
[b] TIMS – thermal ionization mass spectrometry.

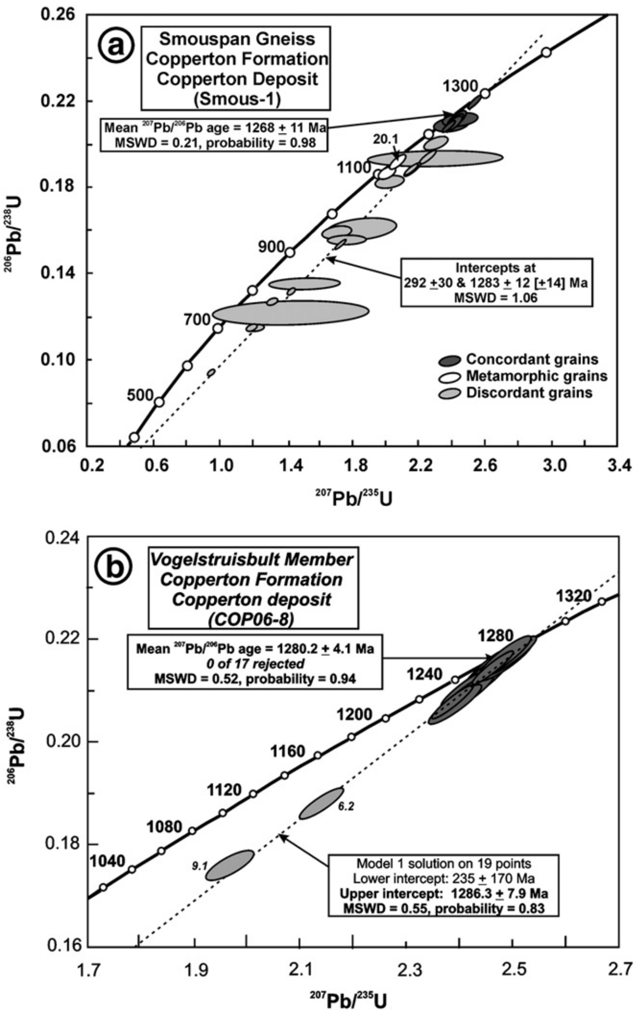

Fig. 7. Geochronology of the host rocks to the Copperton deposit. U-Pb concordia diagrams for zircons from the host gneisses to the Copperton deposit, Copperton Formation, Areachap Group. a. The footwall Smouspan Gneiss of dacitic composition (sample Smous-1). b. The metasedimentary hanging-wall Vogelstruisbult Member of varying composition (sample COP06-8).

analyses with low Th/U ratios of 0.1 or less (analyses 6.1 and 20.1, Table A9) of unzoned overgrowths, have $^{207}Pb/^{206}Pb$ ages of 1124 ± 65 Ma and 1143 ± 20 Ma respectively, the latter being only 1% discordant.

Zircons extracted from the sample of the Vogelstruisbult Member are predominantly subhedral, small (>100 μm), with complex zonation patterns which differ from the simple concentric patterns found in the zircons of the Smouspan Gneiss. Cornell and Pettersson (2007) reported similar zircon morphologies with bright oscillatory zoned inner domains that were broken and then overgrown and invaded by dark rims. The zircons have little common Pb compared to the variable and high common Pb in the Smouspan Gneiss zircons (Table A10). The U and Th contents and Th/U ratios of the zircons consistently fall within a small range, with the latter ranging between 0.50-0.71 and are generally higher and more consistent than those in the Smouspan Gneiss zircons, which vary between 0.08 and 1.23.

The zircons are, in general, concordant (Fig. 7b; Table A10), and yield an upper intercept age of 1286.3 ± 7.9 Ma that is almost identical to that of the footwall Smouspan Gneiss. A mean $^{207}Pb/^{206}Pb$ age of 1280.2 ± 4.1 Ma is obtained on two of the most concordant analyses (Fig. 7b). Cornell and Pettersson (2007) reported an upper intercept age of 1282 ± 45 Ma from their metasedimentary sample of the Vogelstruisbult Member.

Both of these ages are within error of that of the Smouspan Gneiss, which suggests derivation of this metasedimentary or metavolcaniclastic gneiss from a provenance of the same age as the intermediate footwall gneiss, and hence deposition of the Copperton Formation, and associated mineralisation, at ~1290-1280 Ma.

5. Discussion

Despite high-grade metamorphism and polyphase deformation, the Copperton massive sulphide orebody and the enclosing PCMA preserve numerous characteristics that permit reconstruction of the original architecture of the deposit as summarized in Fig. 8. The figure is given as a modified stratigraphic column, which has been related to the bimodal-felsic type of VMS deposit as illustrated by Galley et al. (2007), and modified from Barrie and Hannington (1999). Essentially, the PCMA may be described as being comprised of a single, large and tabular massive sulphide lens, underlain by a well-developed footwall alteration zone and overlain by a number of characteristic cap rock lithologies.

The Smouspan Gneiss, comprising the floor to the ore-bearing PCMA, is regarded as a voluminous succession of dacitic volcanic rocks (Theart et al., 1989). The mild effects of epidote + calcite alteration observed in the Smouspan Gneiss (Fig. 4) are regarded as been related to retrograde metamorphism and associated fluid flow, and thus unrelated to ore formation. As such, the Smouspan Gneiss was unlikely to have been the cause of hydrothermal fluid circulation associated with the Copperton deposit as considerably more hydrothermal alteration, apart from the mild epidote + calcite diagenetic alteration, would have been expected along the margins of the Smouspan Gneiss unit if it did drive a hydrothermal cell associated with VMS mineralisation genesis.

The stratigraphic footwall of the massive sulphide lens is marked by the geochemical effects of pervasive hydrothermal alteration (Figs. 4 and 8), as previously noted by Schade et al. (1989), Theart (1985) and Theart et al. (1989). Phlogopite- cordierite-, gedrite- and tourmaline-bearing gneisses commonly contain disseminated sulphides and bear the hallmark of intensive chloritization and less important sericitization, typically associated with the footwall of VMS deposits (Large et al., 2001). Importantly, this altered succession of the PCMA is in gradational contact with the Smouspan Gneiss. The flat, tabular nature of the footwall alteration zone, its apparently conformable gradation into the unaltered Smouspan Gneiss and the close geochemical relation between the alteration zone and the Smouspan Gneiss may be attributed to: (i) deformation, (ii) a footwall alteration zone that was originally semi-conformable or sheet-like with respect to the massive sulphide lens, as is the case for numerous VMS deposits hosted in volcaniclastic rocks, such as Thalanga or Rosebury (Gifkins et al., 2005), (iii) footwall alteration that was constrained to a relatively permeable unit (such as the volcaniclastic and sedimentary rocks of the PCMA as opposed to the dacitic volcanic rocks of the Smouspan Gneiss) (e.g., Doyle and Allen, 2003), or (iv) a combination of the above. Extensive deformation and metamorphism prohibit distinction between these alternatives. Importantly, the succession of altered lithologies of the PCMA below the massive sulphide lens is too thin to have been the source for all the metals in the Copperton deposit. This is attributed tentatively to structural attenuation of the footwall alteration zone during intense deformation.

The thin and complex succession of unusual lithotypes above the massive sulphide orebody may be interpreted as a former cap rock assemblage. This cap rock assemblage includes a fine-grained pyritic quartzite, thought to represent sulphide-bearing metachert, a carbonate-sulphate-rich lithology, likely representing a former carbonate and sulphate cap rock, and a manganese-rich magnetite zone (Fig. 8), regarded as the metamorphic equivalent of low-temperature Fe-Mn oxyhydroxide precipitates. These lithologies are typical cap rocks to VMS deposits (Franklin et al., 2005; Galley et al., 2007). The lithologies occurring immediately above the massive sulphide lens and that comprise the uppermost part of the PCMA are regarded as metamorphosed equivalents of this entire suite of cap rocks.

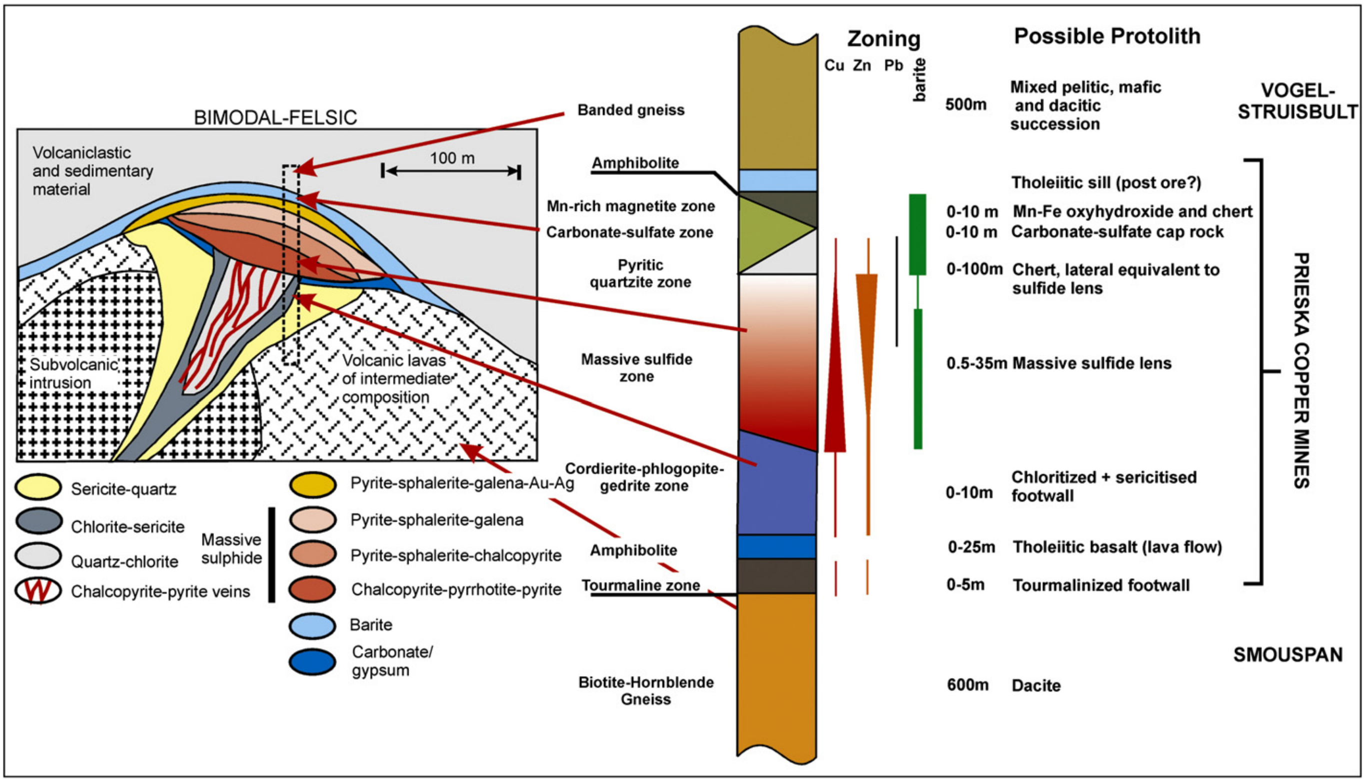

Fig. 8. Architecture of the Copperton deposit as related to a simplified model of a bimodal felsic type of VMS deposit. The Copperton deposit has a volcanic footwall succession of intermediate composition, an altered footwall to the massive sulphide orebody, prominent cap rocks and a sedimentary hanging wall. This architecture is deduced from descriptions in Middleton (1976), Theart (1985), Uiterwyk and Frick (1985), and Wagener and Van Schalkwyk (1986). The bimodal-felsic type of VMS deposit is from Galley et al. (2007), modified after Barrie and Hannington (1999).

The metavolcanic and metasedimentary succession of the Vogelstruisbult Member, by contrast, is interpreted as cover sequence. Its deposition either followed on or even caused the termination of hydrothermal fluid flow and ore formation, as, due to the lack of hydrothermal alteration in these rocks (Fig. 4), hydrothermal activity waned and was either terminated by the time sedimentation / volcanic activity of the Vogelstruisbult Member commenced. The lack of strong hydrothermal alteration without an abrupt break in intensity into the hanging wall of the massive sulphide orebody is a factor that argues against a replacement-type origin for the Copperton deposit.

The very close similarity in ages (Fig. 7; Tables A9 and A10; Cornell and Pettersson, 2007) between the footwall dacitic Smouspan Gneiss and the hanging-wall Vogelstruisbult Member support the VMS model for the Copperton deposit with the hydrothermal fluid flow causing the massive sulphide mineralisation terminated by volcaniclastic and sedimentary deposits derived from the same, or a similar source to that which gave rise to the volcanic footwall. The Copperton deposit was formed at approximately 1280–1290 Ma.

The Copperton deposit has many important characteristics of the bimodal-felsic VMS type in the classification scheme of Barrie and Hannington (1999), including the abundance of volcaniclastic and/or compositionally immature metasedimentary rocks of intermediate to mafic provenance, with associated but quantitatively minor mafic volcanic units, but also the development of a prominent chloritic and sericitic footwall alteration zone underlain by a prominent volcanic dacitic unit. In addition, the barite-, Zn- and Ag-rich nature of the Copperton deposit is typical of bimodal-felsic type VMS deposits (Barrie and Hannington, 1999).

Furthermore, a number of characteristics of the Copperton deposit may be used to invoke a chimney-type VMS system. These include: (i) distinct metal zonation of the orebody, which has been identified as a characteristic of chimney-type VMS deposits (Solomon et al., 2004), (ii) the presence of distinctive cap rocks wherein sulphide-silicate-sulphate mounds occur in intimate association with low-temperature hydrothermal Fe-Mn oxyhydroxide precipitates and chert or jasper deposits and may also be capped by an impermeable carbonate layer (Galley et al., 2007), and (iii) the close spatial association between a footwall alteration zone and massive sulphide lens and an abundance of barite (Solomon et al., 2004). Subsea-floor replacement deposits (Doyle and Allen, 2003) are distinguished by five criteria: (1) mineralised intervals are enclosed within rapidly emplaced volcanic or sedimentary facies, (2) relics of the host facies occur within the mineral deposit, (3) replacement fronts occur between the mineral deposit and the host lithofacies, (4) the mineral deposit is discordant to bedding, and (5) strong hydrothermal alteration continues into the hanging wall without an abrupt break in intensity. Criteria 1–3 are diagnostic, whereas criteria 4 and 5 may suggest replacement but are not alone diagnostic (Doyle and Allen, 2003). The strongly deformed and highly metamorphosed nature of the Copperton deposit is such that many of the original sedimentary or igneous features have been obliterated. Nevertheless there is no evidence for replacement fronts between the mineral deposit and host lithofacies, the deposit does not seem to be discordant to bedding, and the Vogelstruisbult Member does not exhibit strong hydrothermal alteration. Relics of the host facies occur within the mineral deposit but this is due to the development of durchbewegung textures during deformation (Vokes, 2000).

The positive $\varepsilon_{Nd(t)}$ values for both the amphibolites and metasedimentary gneisses from the Copperton deposit (Fig. A4; Table A5) denote derivation of the protolith magmas and related volcaniclastic material and derived sediments from a mantle source. A minor crustal contribution is evident in the enrichment of the amphibolites and gneisses in Th, U, Pb and the large ion lithophile elements along with enrichment of the light rare earth elements relative to the heavy rare earth elements. $\varepsilon_{Nd(t)}$ values close to zero also denote a degree of crustal assimilation. The Copperton deposit was thus formed in a continental island arc setting.

6. Conclusion

The Copperton deposit is identified as a very large example of a chimney-type VMS deposit in a bimodal-felsic environment. It formed during the evolution of the Mesoproterozoic Areachap volcanic arc during a time that this arc was evidently submerged, similar to the current setting of the modern Tonga-Kermadec volcanic arc (De Ronde et al., 2005). The massive sulphide orebody likely formed as a mound on the seafloor, with metals and sulphide leached from the underlying footwall rocks by hydrothermally modified seawater. The cause of hydrothermal fluid circulation and the source of heat to drive the fluids may possibly have been granitoid intrusions in the area. The Smouspan Gneiss, despite being the stratigraphic footwall, likely represents a dacitic volcanic pile. The massive sulphide is associated with distinctive cap rocks and is overlain by a thick volcanosedimentary hanging wall succession.

Although similar in several important attributes, such as broad geological setting, age, metal tenor, and sulphide sulphur isotope values (Bailie et al., 2010b), the Copperton deposit is distinctly different from the other Zn-Cu deposits of the Areachap Group. The latter are not only much smaller, but also lack a footwall alteration zone that is as prominent as the PCMA. Cap rocks, so well developed at Copperton, are conspicuously absent from all the other Areachap Group deposits (Bailie, 2008). Barite, omnipresent at Copperton, has been observed in very minor amounts at the Kantienpan deposit (Ghavami-Riabi, 2006; Stüeken, 2006; Fig. 2), and has not been described from any of the other deposits (Gorton, 1981; Scheepers, 1989; Stüeken, 2006; Voet and King, 1986). Furthermore, metal zonation observed at Copperton appears absent from the smaller deposits (Scheepers, 1989; Voet and King, 1986), though this may also be related to a lack of data density. Combined, these observations may be used to suggest that all smaller Zn-Cu deposits of the Areachap Group (Fig. 2) are brine pool type deposits, or possibly replacement-type deposits in certain cases, as opposed to chimney-type deposits.

These differences provide a number of tools that may be applied to prioritize targets during future exploration efforts in the Areachap Belt. Criteria which may be used to distinguish ore-forming environments akin to the Copperton deposit from reconnaissance geological evidence include: (i) the abundance of rocks of felsic and intermediate composition, such as the voluminous Smouspan Gneiss at Copperton, (ii) the pervasive and intense chloritic and/or sericitic alteration of footwall rocks, (iii) the presence of distinctive cap rocks, especially sulphide-bearing metacherts, and (iv) the presence of barite in surficial gossans.

Acknowledgements

The friendly and helpful folk at PRISE, the Research School of Earth Sciences at the Australian National University (ANU), Canberra, Australia, particularly Richard Armstrong and Gael Watson, are thanked for all their help, guidance, assistance and hospitality during the SHRIMP zircon geochronological work undertaken there. Sifiso Zwane and Benny Chisonga are gratefully thanked for sample preparation for the geochronological study. Reviewers Alan Galley, George Hudak, and Associate Editor Paul Spry are thanked for constructive criticism and reviews of earlier versions of this manuscript that helped improved it. This research was funded by a national research fund (NRF) bursary granted to JG (FA 2004050300016) along with funding from the Faculty of Science, University of Johannesburg.

Appendix

Table A1
Petrography of lithologies from the Copperton deposit, Areachap Group (after Bailie et al., 2010a).

Lithology	Samples	Mineralogy
Copperton core D378		
Smouspan Member		
Feldspathic amphibole gneiss	D378-1, 2, 3, 4, 5, 6, 8, 10	hornblende, plagioclase (An_{58-78}), biotite, quartz, orthoclase, sphene, magnetite, ilmenite, apatite, zircon ± riebeckite ± pargasite ± sillimanite ± phlogopite ± chlorite ± pyrite ± calcite
Feldspathic amphibole gneiss	Smous-1	hornblende, plagioclase (An_{63-74}), biotite, quartz, orthoclase, sphene, magnetite, ilmenite, zircon, apatite ± sericite
Prieska Copper Mines Assemblage (PCMA)		
Amphibolite	D378-13	hornblende, plagioclase, quartz ± biotite ± muscovite ± glaucophane ± schorl
Biotite gneiss	D378-18, 21, 27, 34	quartz, biotite, plagioclase (An_{45-60}), magnetite, muscovite, sillimanite ± monazite ± hornblende ± cordierite ± K-feldspar
Vogelstruisbult Member		
Biotite amphibole gneiss	D378-44, 48	quartz, biotite, hornblende, orthoclase, plagioclase, cordierite, chlorite ± sillimanite ± muscovite
Feldspathic biotite amphibole gneiss	D378-47	quartz, plagioclase, biotite, hornblende ± muscovite
Feldspathic amphibole gneiss	D378-46, 49, 50	hornblende, cummingtonite, plagioclase (An_{73-85}), quartz, chlorite, phlogopite, orthoclase, cordierite ± calcite ± diopside ± titanite ± epidote
Copperton core D352		
Smouspan Member		
Biotite-amphibole gneiss	D352-10	hornblende, richterite, quartz, biotite, plagioclase (An_{55-66}), sillimanite, magnetite, pyrite
Vogelstruisbult Member		
Feldspathic amphibole gneiss (metasediment)	D352-4	hornblende, plagioclase (An_{45-67}), biotite, quartz, orthoclase, sphene, magnetite, ilmenite, apatite, zircon ± cummingtonite, pargasite ± ferroglaucophane ± riebeckite ± actinolite
Amphibole gneiss (metasediment)	D352-5	hornblende, plagioclase (An_{60-67}), biotite, quartz, orthoclase, magnetite, ilmenite, zircon, apatite ± actinolite
Amphibolite	D352-6	hornblende, plagioclase (An_{45-65}), quartz, biotite, magnetite, ilmenite ± cummingtonite ± wollastonite ± phillipsite ± diopside ± cordierite

As far as possible sampling was undertaken on each mesoscopically recognizable lithological unit so as to avoid clustering and compositional bias. Polished thin sections were prepared for all samples. Results were used to arrive at a lithological classification following the recommendations of the British Geological Survey (BGS) (Robertson, 1999).
Abbreviations: f/w: footwall; h/w – hanging wall.

Table A2
Average major element geochemistry of lithological units from the Copperton deposit, Areachap Group (after Bailie et al., 2010a).

Lithology	Samples	SiO_2 [b]	TiO_2	Al_2O_3	Fe_2O_3	MnO	MgO	CaO	Na_2O	K_2O	P_2O_5
Copperton core D378											
Smouspan Member											
Feldspathic amphibole gneiss	D378-1, 2, 3, 4, 6, 8, 10	65.05	0.55	15.14	4.90	0.09	1.45	5.71	4.10	0.63	0.24
Biotite gneiss	D378-5	66.07	0.50	14.77	4.74	0.07	1.17	5.23	3.75	1.25	0.21
Amphibole biotite gneiss	D378-12	76.60	0.19	11.65	3.16	0.08	1.71	2.71	2.62	0.98	0.03
PCMA											
Amphibolite	D378-13	47.59	1.01	13.86	11.59	0.29	7.02	11.99	3.32	bdl[a]	0.08
Biotite gneiss	D378-16, 18–22, 24, 25, 27	68.60	0.36	12.37	5.36	0.10	3.58	0.26	2.43	2.40	0.07
Vogelstruisbult Member											
Biotite amphibole gneiss	D378-44, 48	74.04	0.17	11.93	2.43	0.05	1.08	1.28	3.23	2.74	0.02
Amphibole gneiss	D378-47	60.80	1.29	13.74	11.41	0.23	2.53	4.99	2.98	1.23	0.63
Biotite amphibole gneiss	D378-46, 49, 50	61.26	1.17	13.82	7.59	0.20	2.49	3.67	3.79	1.59	0.56
Copperton core D352											
Smouspan Member											
Biotite amphibole gneiss	D352-10	52.48	1.45	13.08	15.65	0.26	5.64	7.28	2.09	0.94	0.32
Vogelstruisbult Member											
Feldspathic amphibole gneiss (metasediment)	D352-4	53.11	1.57	14.36	16.74	0.20	4.19	5.98	2.88	0.20	0.19
Amphibole gneiss (metasediment)	D352-5	52.77	1.74	14.28	17.19	0.17	4.06	6.14	3.16	0.19	0.19
Amphibolite	D352-6	46.73	0.98	15.72	14.12	0.19	9.11	10.17	2.46	0.22	0.07

Notes: Sample powders of the required analytical fineness were prepared in a Cr-steel Siebtechnik vibratory disc mill at the facilities of the Department of Geology, University of Johannesburg (UJ). Whole rock major element geochemical analyses on fusion beads (using a 50/50 lithium metaborate / lithium tetraborate mixture as flux). Measurements for Copperton core D378 by XRF analysis using the methodology of Norrish and Hutton (1969) on a Phillips PW2540 spectrometer at the Central Analytical Facility of the Faculty of Science, University of Johannesburg, for core D352 done by ICP-OES analysis by Acme Laboratories, Vancouver Canada. Analytical errors for each oxide on XRF are approximately 2% (relative), but higher for SiO_2 and Al_2O_3. Absolute errors (1 std. deviation) (in wt %) are as such: SiO_2 – 0.02, TiO_2 – 0.01, Al_2O_3 – 0.08, Fe_2O_3 – 0.12, MnO – 0.01, MgO – 0.08, CaO – 0.04, Na_2O – 0.09, K_2O – 0.03, P_2O_5 – 0.01. Detection limits (in wt%) for the major oxides are as such: SiO_2 – 0.03, TiO_2 – 0.006, Al_2O_3 – 0.02, Fe_2O_3 – 0.02, MnO – 0.03, MgO – 0.08, CaO – 0.01, Na_2O – 0.08, K_2O – 0.004, P_2O_5 – 0.04. Detection limits for ICP-MS analysis (%) are as such: SiO_2 – 0.01, TiO_2 – 0.01, Al_2O_3 – 0.03, Fe_2O_3 – 0.04, MnO – 0.01, MgO – 0.01, CaO – 0.01, Na_2O – 0.01, K_2O – 0.04, P_2O_5 – 0.01.
[a] bdl — below detection limits.
[b] All data are in weight percent (wt.%).

Table A3
Trace element geochemistry of lithological units from the Copperton deposit, Areachap Group (after Bailie et al., 2010a).

Lithology	Rb[c]	Ba	Sr	Pb	Zr	Hf	Th	Nb	Ta	U	Y	Sc	La	Ce	Ni	Co	Cr	Cu	Zn	V
Copperton core D378																				
Smouspan Member																				
Feldspathic amphibole gneiss	19	496	335	6	127	1.0	6.6	9	n.d.	n.d.	31	n.d	30.7	55.3	13	7	181	10	49	45
Biotite gneiss	29	1301	355	5	140	2.3	8.0	9	n.d.	n.d.	33	n.d	34.2	64.8	26	6	220	14	52	54
Hornblende biotite gneiss	20	511	145	2	159	10.6	9.2	7	n.d.	n.d	25	n.d	32.3	62.0	18	3	308	50	36	18
PCMA																				
Amphibolite	5	47	120	n.d.	53	n.d.	1.0	4	n.d.	n.d.	24	n.d	n.d.	3.1	124	42	320	13	123	200
Biotite gneiss	60	1052	77	3	107	3.2	7.0	9	n.d.	n.d	36	n.d.	26.0	50.7	16	6	245	25	78	41
Vogelstruisbult Member																				
Biotite amphibole gneiss	71	4197	183	716	304	64.9	37.2	9	n.d.	n.d.	18	n.d.	41.1	101.5	25	1	203	166	193	17
Biotite amphibole gneiss	35	392	246	26	79	n.d.	2.8	5	n.d.	n.d.	33	n.d.	15.0	12.0	16	7	153	16	132	58
Feldspathic amphibole gneiss	33	250	237	4	82	n.d.	1.4	6	n.d.	n.d.	41	n.d.	10.0	13.0	14	10	104	16	163	67
Copperton core D352																				
Smouspan Member																				
Biotite amphibole gneiss	31	278	209	8	46	1.8	1.0	2	0.1	0.2	30	44	8.8	19.9	6	26	n.d.	5	105	363
Vogelstruisbult Member																				
Biotite amphibole gneiss	54	2385	210	31	162	2.4	7.3	8	n.d.	n.d.	34	n.d.	20.1	51.0	15	7	120	13	207	49
Amphibole gneiss	35	392	246	26	79	n.d.	2.8	5	n.d.	n.d.	33	n.d.	14.9	n.d.	16	7	153	16	132	58
Biotite amphibole gneiss	73	5199	168	680	321	53.0	31.3	8	n.d.	n.d.	12	n.d.	46.9	100.4	17	0	185	143	246	15

[a]Averages are for samples listed in Table A2.
[b]n.d. – not determined or below detection limits.
[c]All data in parts per million (ppm).
Notes: Sample powders of the required analytical fineness were prepared in a Cr-steel Siebtechnik vibratory disc mill at the facilities of the Department of Geology, University of Johannesburg (UJ). Trace element analyses done by ICP-MS at Acme Laboratories, Vancouver, Canada. Mean detection limits (in ppm) are: Cu – 0.1, Pb – 0.1, Zn - 1, Ni – 0.1, Co – 0.2, U – 0.1, Th – 0.2, Sr – 0.5, Sb – 0.1, V - 8, P – 100, Ba – 1, Ti – 100, K – 100, Zr – 0.1, Sc – 1, Y – 0.1, Hf – 0.1, Rb – 0.1, Ta – 0.1, Nb – 0.1. Errors (1σ variation) are within 1% of the results.

Table A4
Rare earth element (REE) geochemistry of lithological units from the Copperton deposit, Areachap Group (after Bailie et al., 2010a).

Lithology	Samples	La[a]	Ce	Pr	Nd	Sm	Eu	Gd	Tb	Dy	Ho	Er	Tm	Yb	Lu
Copperton core D352															
Smouspan Member															
Biotite amphibole gneiss	D352-10	8.8	19.9	2.8	13.4	3.7	1.7	4.3	0.8	4.9	1.1	3.4	0.5	3.1	0.5
Vogelstruisbult Member															
Feldspathic amphibolite	D352-4	7.9	16.8	2.3	10	3.1	1.4	3.4	0.6	4.1	0.9	2.4	0.4	2.4	0.4
Amphibole gneiss	D352-5	7.2	16.6	2.3	11.7	3.5	1.2	3.7	0.7	4.4	0.9	2.8	0.4	2.7	0.5
Amphibolite	D352-6	4.4	9.9	1.4	7.2	1.6	0.7	1.8	0.3	2.3	0.5	1.4	0.2	1.4	0.2

Notes: Sample powders of the required analytical fineness were prepared in a Cr-steel Siebtechnik vibratory disc mill at the facilities of the Department of Geology, University of Johannesburg (UJ). Trace element analyses done by ICP-MS at Acme Laboratories, Vancouver, Canada. Mean detection limits (in ppm) are: La – 0.5, Ce – 0.5, Pr – 0.02, Nd – 0.4, Sm – 0.1, Eu – 0.05, Gd – 0.05, Tb – 0.01, Dy – 0.05, Ho – 0.05, Er – 0.05, Tm – 0.05, Yb – 0.05, Lu – 0.01. Errors (1σ variation) are within 1% of the results.
[a] All data in parts per million (ppm).

Table A5
Sm-Nd isotopes and model ages for the Copperton deposit (after Bailie et al., 2010a).

Sample	Lithology	Sm (ppm)	Nd (ppm)	Sm/ Nd	$^{147}Sm/^{144}Nd$	$^{143}Nd/^{144}Nd_{(0)}$	2σ	$^{143}Nd/^{144}Nd_{(t)}$	$\varepsilon_{Nd(t)}$	$f^{(Sm/Nd)}$	T_{CHUR} (Ga)	T_{DM} (Ga) DePaolo (1981)
Copperton (this study)												
SM5-35	Biotite gneiss	2.07	7.64	0.27	0.1639	0.512469	9	0.511085	2.10	−0.17		1.744
D378-12	Amphibole biotite gneiss	5.43	27.66	0.20	0.1187	0.512133	12	0.511130	2.98	−0.40	0.987	1.456
VAX20-9	Hornblende biotite gneiss	6.73	32.38	0.21	0.1257	0.512208	11	0.511146	3.30	−0.36	0.923	1.442
VAX20-34	Amphibolite	3.47	10.63	0.33	0.1975	0.512863	10	0.511195	4.26	0.00		1.644
VAX20-46	Amphibolite	5.25	15.62	0.34	0.2033	0.512928	11	0.511211	4.57	0.03		1.616
Copperton (from Cornell et al., 1986)												
D303-56	Metadacite gneiss (Smouspan)	4.76	22.66	0.21	0.1269	0.51215	10	0.511078	1.96	−0.35	1.065	1.563
D303-84	Metadacite gneiss (Smouspan)	4.94	23.30	0.21	0.1282	0.51314	10	0.512057	2.13	−0.35		
D303-501	Intermediate paragneiss (VSB [a])	16.86	60.32	0.28	0.1691	0.51252	10	0.511092	2.24	−0.14		1.772
D303-590	Metapelitic gneiss (VSB)	6.25	31.97	0.20	0.1180	0.51208	10	0.511082	2.04	−0.40	1.082	1.531
D303-624	Basic paragneiss (VSB)	2.33	9.47	0.25	0.1489	0.51235	10	0.511093	2.25	−0.24		1.620
D303-643	Arkosic gneiss (VSB)	2.12	9.28	0.23	0.1378	0.51229	10	0.511126	2.90	−0.30		1.506
D303-743	Laminated amphibolite (VSB)	2.69	8.02	0.33	0.2026	0.51297	10	0.511259	5.51	0.03		
D303-746	Laminated amphibolites (VSB)	2.52	7.63	0.33	0.1997	0.51288	10	0.511193	4.22	0.02		1.726
D303-756b	Calc-silicate band (VSB)	2.54	7.64	0.33	0.2009	0.51286	10	0.511163	3.63	0.02		2.161
D303-756d	Amphibolite band (VSB)	2.22	6.83	0.32	0.1965	0.51284	10	0.511181	3.98	0.00		1.754
D352-29	Intermediate amphibolite (VSB)	4.32	14.68	0.29	0.1779	0.51266	10	0.511157	3.52	−0.10		1.613
V38-3	Metapelite (VSB)	6.08	32.37	0.19	0.1137	0.51204	10	0.511080	2.00	−0.42	1.097	1.524

Notes: For Nd-isotope analyses, sample powders were prepared in an agate mill using the same laboratory facilities at UJ. The Nd isotopic compositions were determined in the radiogenic isotope facility of the Research School of Earth Sciences, the Australian National University, Canberra, using a Finnigan MAT 261 multi-collector thermal ionization mass spectrometer. Single $HF/HNO_3/HClO_4$ dissolutions of ~350 mg of whole rock powders, spiked with approximately 0.20 to 0.30 g of Sm-Nd ANU-1 spike, were used for measuring Nd isotopic compositions. The $^{143}Nd/^{144}Nd$ ratios were corrected for fractionation using $^{146}Nd/^{144}Nd = 0.72190$ and normalized to $^{143}Nd/^{144}Nd = 0.511840$ for the La Jolla standard. A value of 0.512638 for $^{143}Nd/^{144}Nd$ is used in the calculation of chondritic reservoir (T_{CHUR}) model ages. T_{DM} (depleted mantle model ages) were calculated based on the depleted mantle model of De Paolo (1981). The samples analysed in this study were compared to the Sm-Nd data published by Cornell et al. (1986) for the Copperton deposit. The time t, used to determine $\varepsilon_{Nd(t)}$ values, is taken to be 1286 ± 8 Ma, from the result of a $^{207}Pb/^{206}Pb$ zircon SHRIMP age obtained for the Smouspan Gneiss, a dacitic metavolcanic unit that is the footwall to the Copperton massive sulphide lens (see section 4 of main text).
[a] VSB = Vogelstruisbult Member. [b] Model ages for samples with $^{147}Sm/^{144}Nd > 0.12 \pm 0.02$ are not included for T_{CHUR} due to giving unrealistic results.

Table A6
Major element geochemistry of lithological units from the Copperton deposit used in the geochronological study.

Lithology	Sample	SiO_2	TiO_2	Al_2O_3	Fe_2O_3	MnO	MgO	CaO	Na_2O	K_2O	P_2O_5 [a]
Banded amphibole gneiss (Vogelstruisbult Mmb)	COP06-8	52.77	1.74	14.28	17.19	0.17	4.06	6.14	3.16	0.19	0.19
Biotite amphibole gneiss (Smouspan Gneiss)	Smous-1	52.48	1.45	13.08	15.65	0.26	5.64	7.28	2.09	0.94	0.32

[a] Measurements by XRF analysis on a Phillips PW2540 spectrometer at the University of Johannesburg. Absolute errors (1 std. deviation) (in wt%) are as such: SiO_2 – 0.02, TiO_2 – 0.01, Al_2O_3 – 0.08, Fe_2O_3 – 0.12, MnO – 0.01, MgO – 0.08, CaO – 0.04, Na_2O – 0.09, K_2O – 0.03, P_2O_5 – 0.01. Detection limits (in wt%) for the major oxides are down to levels of 0.1 wt% at best, and are as such: SiO_2 – 0.03, TiO_2 – 0.006, Al_2O_3 – 0.02, Fe_2O_3 – 0.02, MnO – 0.03, MgO – 0.08, CaO – 0.01, Na_2O – 0.08, K_2O – 0.004, P_2O_5 – 0.04.

Table A7
Trace element geochemistry of the samples from the Copperton deposit used in the geochronological study.

Sample	Rb	Ba	Sr	Pb	Zr	Hf	Th	Nb	Ta	U	Y	Sc	La	Ce	Ni	Co	Cr	Cu	Zn	V [a]
COP06-8	6	68	331	47	37	1.3	0.6	2.2	0.1	0.2	27	n.d.	7.2	16.6	6	38	n.d.	7	34	315
Smous-1	31	278	209	8	46	1.8	1	2.1	0.1	0.2	30	n.d.[b]	8.8	19.9	6	26	n.d	5	105	363

[a] All data in parts per million (ppm). Trace element analyses done by ICP-MS analysis undertaken by Acme Laboratories, Vancouver, Canada. Mean detection limits (in ppm) are: Cu — 0.1, Pb — 0.1, Zn — 1, Ni — 0.1, Co — 0.5, U — 0.1, Th — 0.1, Sr — 0.5, Sb — 0.1, V — 5, Ba — 0.5, Zr — 0.5, Sc — 1, Y — 0.1, Hf — 0.5, Rb — 0.5, Ta — 0.1, Nb — 0.5. Errors (2σ variations) are within 1% of the results.
[b] n.d. — not detected or below detection limits.

Table A8
Rare earth element (REE) geochemistry of the samples from the Copperton deposit used in the geochronological study.

Lithology	La	Ce	Pr	Nd	Sm	Eu	Gd	Tb	Dy	Ho	Er	Tm	Yb	Lu[a]	ΣREE	Ce/Ce*	Eu/Eu*	$(Gd/Yb)_N$	$(La/Yb)_N$
COP06-8	7.2	16.6	2.25	11.7	3.5	1.2	3.7	0.7	4.43	0.9	2.8	0.4	2.7	0.5	58.56	0.99	0.98	1.12	1.81
Smous-1	8.8	19.9	2.8	13.4	3.7	1.7	4.3	0.8	4.9	1.1	3.4	0.5	3.1	0.5	68.73	0.96	1.29	1.12	1.93

[a] All data in parts per million (ppm). Trace element analyses done by ICP-MS analysis undertaken by Acme Laboratories, Vancouver, Canada. Mean detection limits (in ppm) are: La — 0.5, Ce — 0.5, Pr — 0.02, Nd — 0.4, Sm — 0.1, Eu — 0.05, Gd — 0.05, Tb — 0.01, Dy — 0.05, Ho — 0.05, Er — 0.05, Tm — 0.05, Yb — 0.05, Lu — 0.01. Errors (2σ variations) are within 1% of the results.

Table A9
SHRIMP U-Pb zircon data for zircons from the Smouspan Gneiss, Copperton deposit (sample Smous-1).

Spot	$\%^{206}Pb_c^a$	ppm U	ppm Th	$^{232}Th/^{238}U$	ppm $^{206}Pb^{*a}$	$^{206}Pb/^{238}U$ age[b]	$^{207}Pb/^{206}Pb$ age[b]	%Discordant	$^{207}Pb^*/^{206}Pb^*$[b]	±%	$^{207}Pb^*/^{235}U$[b]	±%	$^{206}Pb^*/^{238}U$[b]	±%	Error correlation[c]
1.1	0.94	676	476	0.73	114	1145 ± 10[a]	1292 ± 17	11	0.08397	0.85	2.25	1.3	0.1943	0.99	0.760
2.1	1.19	861	444	0.53	137	1083 ± 10	1195 ± 52	9	0.0799	2.6	2.015	2.8	0.1829	1.00	0.354
4.1	2.35	723	447	0.64	99	932.6 ± 9.2	1237 ± 81	25	0.0816	4.1	1.752	4.3	0.1557	1.06	0.250
6.1	2.77	217	17	0.08	30.5	953 ± 10	1124 ± 65	15	0.0771	3.2	1.694	3.4	0.1593	1.14	0.331
7.1	0.23	967	1086	1.16	174	1222 ± 11	1262.1 ± 9.1	3	0.0827	0.47	2.38	1.1	0.2088	0.98	0.903
8.1	0.93	729	507	0.72	133	1232 ± 11	1267 ± 17	3	0.08291	0.89	2.407	1.3	0.2105	0.99	0.744
9.1	2.79	879	77	0.09	164	1237 ± 11	1289 ± 51	4	0.0838	2.6	2.446	2.8	0.2116	1.01	0.360
10.1	1.39	1561	1517	1.00	172	769.3 ± 7.1	1071 ± 24	28	0.0751	1.2	1.312	1.6	0.1267	0.97	0.626
11.1	2.32	1700	1881	1.14	171	699.5 ± 6.5	1062 ± 25	34	0.07477	1.2	1.182	1.6	0.1146	0.99	0.624
12.1	1.12	2114	499	0.24	172	576.5 ± 5.3	1000 ± 23	42	0.07252	1.1	0.935	1.5	0.09355	0.97	0.656
13.1	0.93	595	392	0.68	104	1180 ± 11	1272 ± 35	7	0.0831	1.8	2.303	2.1	0.2009	1.01	0.492
14.1	0.04	366	269	0.76	69.3	1283 ± 12	1277 ± 11	0	0.08332	0.55	2.53	1.2	0.203	1.03	0.883
15.1	0.30	1693	753	0.46	192	796.4 ± 7.2	1162 ± 17	31	0.07859	0.85	1.425	1.3	0.1315	0.96	0.748
16.1	0.62	764	208	0.28	124	1106 ± 10	1136 ± 31	3	0.0776	1.5	2.002	1.8	0.1872	1.01	0.547
17.1	0.94	655	411	0.65	107	1116 ± 10	1269 ± 18	12	0.083	0.91	2.164	1.4	01891	1.00	0.736
18.1	6.45	1095	154	0.15	136	817.1 ± 9.4	1213 ± 180	33	0.0807	9.2	1.5	9.3	0.1351	1.22	0.131
19.1	0.39	676	475	0.73	110	1114 ± 10	1259 ± 13	12	0.08257	0.68	2.148	1.2	0.1886	0.99	0.824
20.1	0.86	725	70	0.10	121	1135 ± 10	1143 ± 20	1	0.07784	1	2.067	1.4	0.1926	0.99	0.699
21.1	1.05	1586	1890	1.23	158	702 ± 6.6	1092 ± 59	36	0.0759	3	1.204	3.1	0.1151	0.99	0.319
22.1	5.36	625	669	1.11	110	1141 ± 14	133 ± 230	15	0.086	12	2.3	12	0.1936	1.33	0.113
23.1	9.66	23	2	0.08	2.65	740 ± 21	1307 ± 420	43	0.085	22	1.42	22	0.1216	2.95	0.135
24.1	20.79	350	231	0.68	61.1	962 ± 18	1278 ± 140	25	0.0834	7.2	1.85	7.5	0.1609	1.99	0.265
25.1	0.24	335	169	0.52	61	1236 ± 12	1267 ± 17	2	0.08291	0.89	2.416	1.4	0.2113	1.03	0.756
26.1	0.62	344	189	0.57	63.2	1242 ± 13	1259 ± 22	1	0.08256	1.1	2.418	1.6	0.2124	1.17	0.723
27.1	1.04	439	196	0.46	79.9	1226 ± 11	1264 ± 52	3	0.0828	2.7	2.392	2.9	0.2095	1.03	0.35
28.1	0.43	967	840	0.90	128	920.7 ± 8.4	1221 ± 15	25	0.08099	0.75	1.714	1.2	0.1535	0.97	0.792

Notes: [a] Pb_c and Pb* indicate the common and radiogenic portions respectively. [b] Common Pb corrected using measured ^{204}Pb. [c] Errors are 1-sigma; Error in standard calibration was 0.22% (not included in above errors but required when comparing data from different mounts). Zircons were concentrated using conventional mineral separation techniques, then hand-picked, mounted in epoxy and polished, prior to analysis using the Sensitive High Resolution Microprobe (SHRIMP), housed at the Research School of Earth Sciences (RSES) at The Australian National University, Canberra, Australia. Details of the methodology applied are given by Williams (1998). Cathodoluminescence (CL) and backscatter electron (BSE) images were collected at the RSES. The standard zircon, FC-1 from the Duluth Complex, U.S.A., with an age of ~1100-1080 Ma, was used as a standard during analysis. Errors in the data tables and figures are at the 68% confidence level (1σ), with final weighted mean ages reported at the 95% confidence level. Decay constants used were 1.55125×10^{-10} (^{238}U) and 9.8485×10^{-10} (^{235}U). Statistical analysis and U-Pb Concordia diagrams were generated using Isoplot (Version 3.00) (Ludwig, 2003).

Table A10
SHRIMP U-Pb zircon data for zircons from the Vogelstruisbult Member, Copperton Formation, Copperton deposit (sample COP06-8).

Spot	$\%^{206}Pb_c^a$	ppm U	ppm Th	$^{232}Th/^{238}U$	ppm $^{206}Pb^{*a}$	$^{206}Pb/^{238}U$ Age[b]	$^{207}Pb/^{206}Pb$ Age[b]	% Discordant	$^{207}Pb^*/^{206}Pb^*$[b]	±%	$^{207}Pb^*/^{235}U$[b]	±%	$^{206}Pb^*/^{238}U$[b]	±%	Error correlation[c]
1.1	0.03	573	398	0.72	106	1260 ± 12 [a]	1288.5 ± 8	2	0.08382	0.41	2.494	1.1	0.2158	1.1	0.932
2.1	0.00	568	331	0.60	101	1217 ± 12	1277.9 ± 7.6	5	0.08337	0.39	2.388	1.1	0.2077	1	0.937
3.1	0.00	648	325	0.52	119	1248 ± 12	1274 ± 12	2	0.08319	0.6	2.451	1.2	0.2137	1	0867
4.1	0.02	710	553	0.81	128	1227 ± 13	1288.3 ± 9.7	5	0.08381	0.5	2.423	1.2	0.2097	1.1	0.916
5.1	0.11	375	213	0.59	66.6	1210 ± 12	1287 ± 11	6	0.08378	0.56	2.384	1.2	0.2064	1.1	0.886
6.2	0.23	284	122	0.44	45.8	1107 ± 11	1264 ± 13	12	0.08278	0.67	2.139	1.3	0.1874	1.1	0.850
7.1	0.00	656	469	0.74	118	1221 ± 12	1284.1 ± 7.1	5	0.08364	0.37	2.406	1.1	0.2086	1	0.944
8.1	0.00	694	469	0.70	127	1243 ± 12	1281.7 ± 6.8	3	0.08353	0.35	2.449	1.1	0.2126	1.1	0.948
9.1	0.53	482	255	0.55	73.1	1043 ± 10	1227 ± 20	15	0.08121	1	1.967	1.5	0.1756	1.1	0.723
10.1	0.00	704	413	0.61	127	1228 ± 12	1270.6 ± 7.3	3	0.08306	0.38	2.404	1.1	0.2099	1	0.941
11.1	0.03	507	320	0.65	92.8	1245 ± 12	1273.7 ± 8.4	2	0.08319	0.43	2.445	1.1	0.2131	1.1	0.925
12.1	0.06	407	223	0.57	74.8	1248 ± 12	1276 ± 10	2	0.08329	0.51	2.453	1.2	0.2136	1.1	0.902
13.1	0.00	525	367	0.72	95.8	1242 ± 13	1272 ± 8	2	0.08312	0.41	2.434	1.2	0.2124	1.2	0.942
14.1	0.27	434	255	0.61	78.9	1235 ± 12	1281 ± 14	4	0.08349	0.71	2.431	1.3	0.2112	1.1	0.833
15.1	0.04	446	279	0.65	83.2	1266 ± 12	1275.9 ± 9.7	1	0.08328	0.5	2.493	1.2	0.2171	1.1	0.907
16.1	0.00	395	257	0.67	70.5	1218 ± 12	1282.7 ± 9.5	5	0.08357	0.49	2.396	1.2	0.2079	1.1	0.910
17.1	0.04	736	517	0.73	137	1265 ± 12	1281.5 ± 8.6	1	0.08353	0.44	2.498	1.1	0.2169	1	0.920
18.1	0.03	809	423	0.54	149	1249 ± 12	1279.8 ± 7.6	2	0.08345	0.39	2.46	1.1	0.2138	1	0.936
19.1	1.73	509	308	0.63	97.4	1275 ± 12	1306 ± 30	2	0.0846	1.5	2.551	1.9	0.2187	1.1	0.571
20.1	0.00	579	413	0.74	108	1263 ± 12	1286.3 ± 7.9	2	0.08373	0.41	2.5	1.1	0.2165	1.1	0.933

[a] Pb_c and Pb* indicate the common and radiogenic portions respectively.
[b] Common Pb corrected using measured ^{204}Pb.
[c] Errors are 1-sigma; Error in standard calibration was 0.22% (not included in above errors but required when comparing data from different mounts).

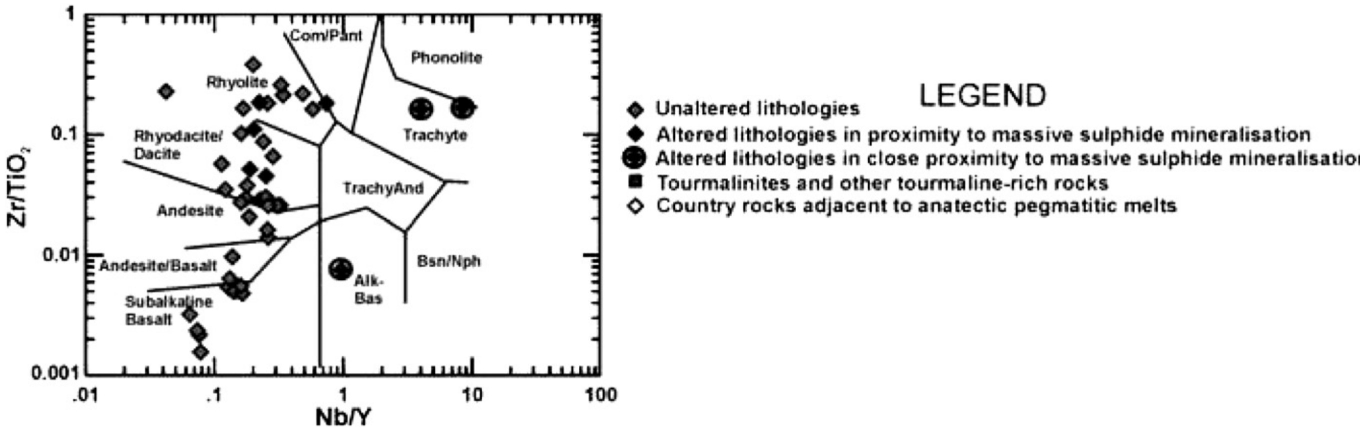

Fig. A1. Trace element geochemical classification of the gneisses and schists of the Copperton deposit using the Zr/TiO_2 vs. Nb/Y plot of Winchester and Floyd (1977). Also included are samples that are in the footwall to the massive sulphide orebody and have been affected by hydrothermal fluid alteration. Figure and data after Bailie et al. (2010a).

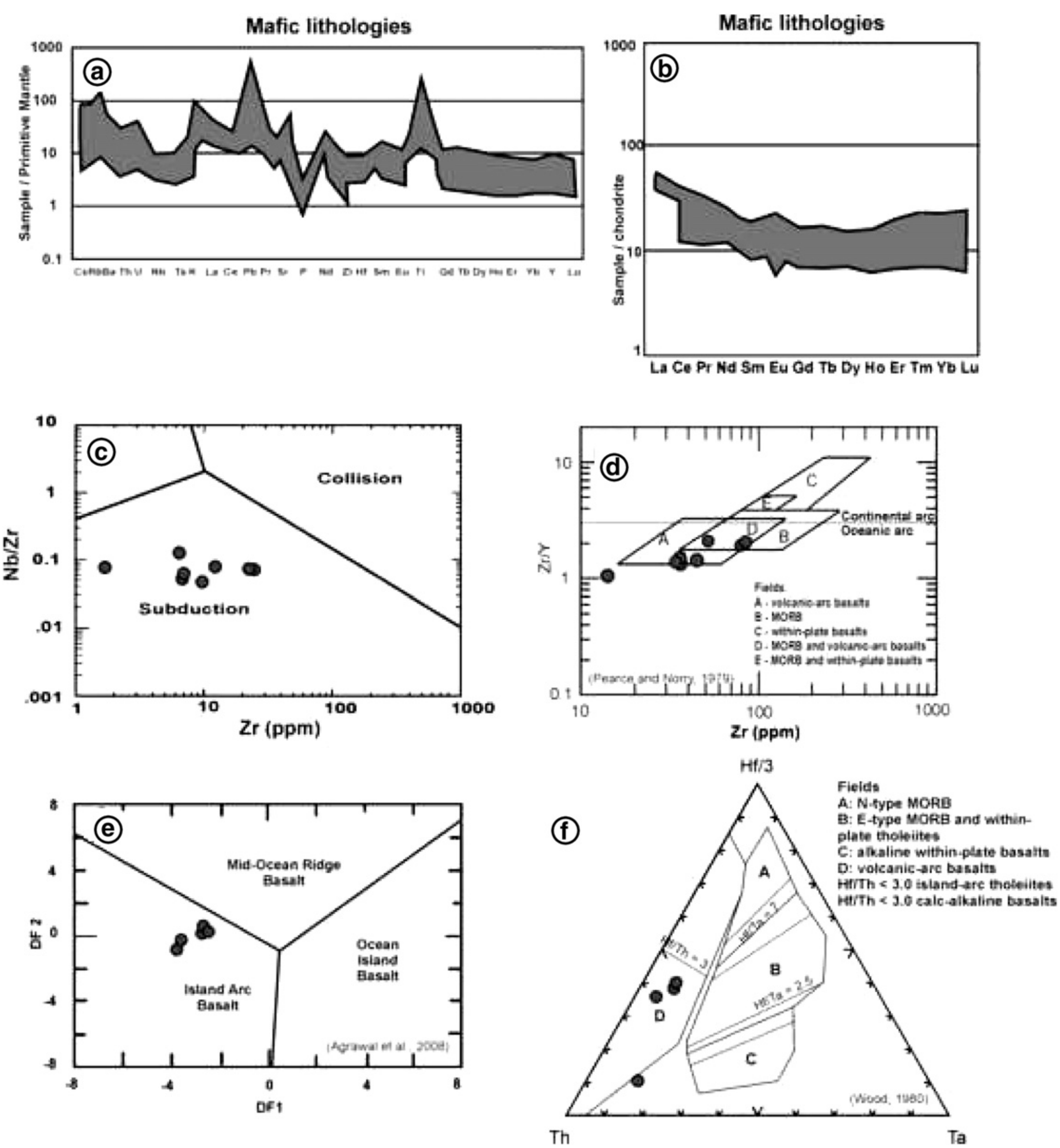

Fig. A2. Trace element characteristics of the lithologies of mafic composition in the Copperton deposit. a. Primitive mantle-normalised trace element (spider) diagram, plotted according to the order of, and normalised according to the values of McDonough et al. (1991). b. Chondrite-normalised rare earth element plot normalised to the chondrite values of Nakamura (1974). c. The Nb/Zr vs. Zr plot to distinguish between subduction-related and collision-related tectonic settings. d. The Zr/Y vs. Zr plot of Pearce and Norry (1979) to discriminate various tectonic settings. e. The immobile trace element discriminant function tectonic setting diagram of Agrawal et al. (2008). f. The Th-Hf/3-Ta ternary tectonic discrimination plot of Wood (1980). Data from Bailie et al. (2010a) and figures modified after Bailie et al. (2010a).

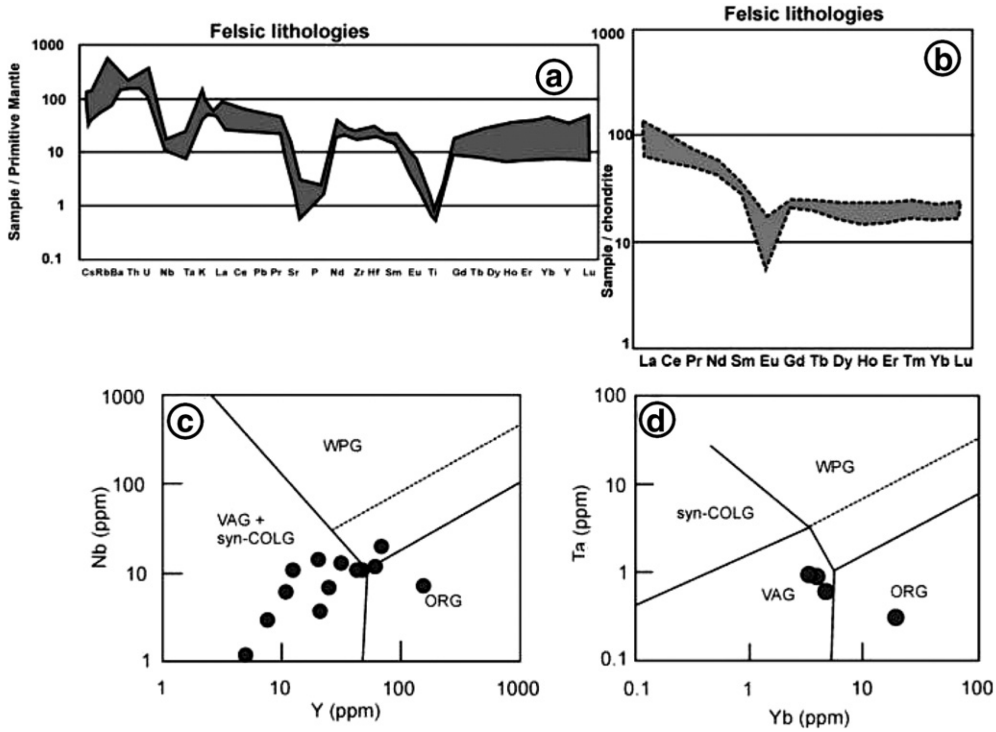

Fig. A3. Trace element characteristics of the lithologies of felsic composition in the Copperton deposit. a. Primitive mantle normalised multi-element trace element (spider) diagram, plotted according to the order of, and normalised according to the values of McDonough et al. (1991). b. Chondrite normalised rare earth element plot normalised to the chondrite values of Nakamura (1974). c and d. The Nb vs. Y and Ta vs. Yb tectonic discrimination diagrams of Pearce et al. (1984) for lithologies of felsic composition. Data from Bailie et al. (2010a) and figures modified after Bailie et al. (2010a).

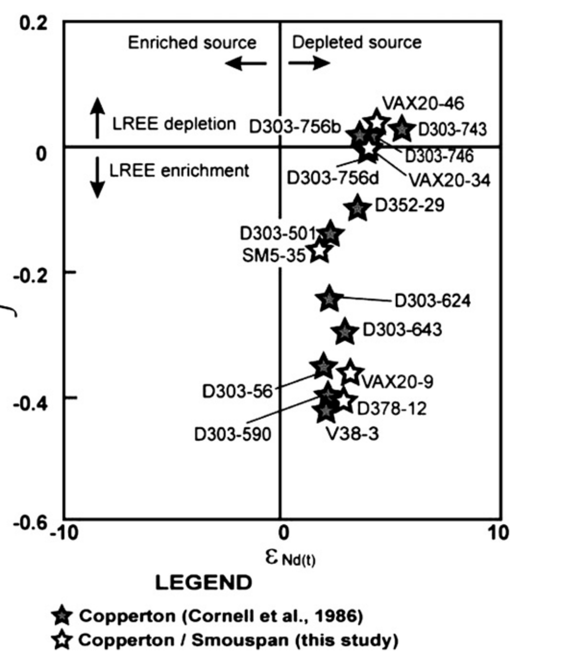

Fig. A4. Sm-Nd isotopic characteristics of the Copperton deposit. f^{Sm-Nd} vs. $\varepsilon_{Nd(t)}$ plot for the Copperton deposit (data from Bailie et al., 2010a; Cornell et al., 1986).

References

Agrawal, S., Guevara, M., Verma, S.P., 2008. Tectonic discrimination of basic and ultrabasic volcanic rocks through log-transformed ratios of immobile trace elements. International Geology Review 50, 1057–1079.

Bailie, R.H., 2008. Mesoproterozoic volcanism, metallogenesis and tectonic evolution along the western margin of the Kaapvaal Craton. Unpublished Ph.D. Thesis, University of Johannesburg, 236 pp.

Bailie, R., Gutzmer, J., Rajesh, H., 2010a. Lithogeochemistry as a tracer of the tectonic setting, lateral integrity and mineralisation of a highly metamorphosed Mesoproterozoic volcanic arc sequence on the eastern margin of the Namaqua Province, South Africa. Lithos 119, 345–362.

Bailie, R., Gutzmer, J., Strauss, H., Stüeken, E., McClung, C., 2010b. Sulfur isotope characteristics of metamorphosed Zn-Cu volcanogenic massive sulfides in the Areachap Group, Northern Cape Province, South Africa. Mineralium Deposita 45, 481–496.

Barrie, C.T., Hannington, M.D., 1999. Classification of volcanic-associated massive sulfide deposits based on host-rock composition. In: Barrie, C.T., Hannington, M.D. (Eds.), Volcanic-associated massive sulfide deposits: Processes and examples in modern and ancient settings. : Reviews in Economic Geology, 8. Society of Economic Geologists, Boulder, Colorado, pp. 1–11.

Barton, E.S., Burger, A.J., 1983. Reconnaissance isotopic investigations in the Namaqua mobile belt and implications for Proterozoic crustal evolution – Upington geotraverse. In: Botha, B.J.V. (Ed.), Namaqualand Metamorphic Complex: Special Publication of the Geological Society of South Africa, 10, pp. 173–191.

Cornell, D.H., 1978. Age and metamorphism of the Copperton Formation, Prieska District. In: Verwoerd, W.J. (Ed.), Mineralization in Metamorphic Terranes: Special Publication of the Geological Society of South Africa, 4, pp. 223–234.

Cornell, D.H., Pettersson, A., 2007. Ion probe zircon dating of metasediments from the Areachap and Kakamas Terranes, Namaqua-Natal Province and the stratigraphic integrity of the Areachap Group. South African Journal of Geology 110, 575–584.

Cornell, D.H., Hawkesworth, C.J., Van Calsteren, P., Scott, W.D., 1986. Sm-Nd study of Precambrian crustal development in the Prieska-Copperton region, Cape Province. Transactions of the Geological Society of South Africa 89, 17–28.

Cornell, D.H., Theart, H.F.J., Humphreys, H.C., 1990a. Dating a collision-related metamorphic cycle at Prieska Copper Mines, South Africa. In: Spry, P.G., Bryndzia, T. (Eds.), Regional Metamorphism of Ore Deposits and Genetic Implications 11. Springer-Verlag, Utrecht, pp. 97–116.

Cornell, D.H., Kröner, A., Humphreys, H., Griffin, G., 1990b. Age of origin of the polymetamorphosed Copperton Formation, Namaqua-Natal Province, determined by single grain zircon dating. South African Journal of Geology 93, 709–716.

Cornell, D.H., Humphreys, H., Theart, H.F.J., Scheepers, D.J., 1992. A collision-related pressure-temperature-time path for Prieska Copper Mine, Namaqua-Natal tectonic Province, South Africa. Precambrian Research 59, 43–71.

Cornell, D.H., Thomas, R.J., Moen, H.F.G., Reid, D.L., Moore, J.M., Gibson, R.L., 2006. The Namaqua-Natal Province. In: Johnson, M.R., Anhaeusser, C.R., Thomas, R.J. (Eds.), The Geology of South Africa: Geological Society of South Africa. Johannesburg / Council for Geoscience, Pretoria, pp. 325–379.

De Paolo, D.J., 1981. Neodymium isotopes in the Colorado Front range and crust-mantle evolution in the Proterozoic. Nature 291, 193–196.

De Ronde, C.E.J., Hannington, M.D., Stoffers, P., Wright, I.C., Ditchburn, R.G., Reyes, A.G., Baker, E.T., Massoth, G.J., Lupton, J.E., Walker, S.L., Greene, R.R., Soong, C.W.R., Ishibashi, J., Lebon, G.T., Bray, C.J., Resing, J.A., 2005. Evolution of a submarine magmatic-hydrothermal system: Brothers volcano, southern Kermadec arc, New Zealand. Economic Geology 100, 1097–1133.

Doyle, M.G., Allen, R.L., 2003. Subsea-floor replacement in volcanic-hosted massive sulfide deposits. Ore Geology Reviews 23, 183–222.

Franklin, J.M., 1993. Volcanic-associated massive sulfide deposits. In: Kirkham, R.V., Sinclair, W.D., Thorpe, R.I., Duke, K.M. (Eds.), Mineral Deposit Modeling: Geological Association of Canada, Special Paper, 40, pp. 315–334.

Franklin, J.M., Lydon, J.W., Sangster, D.F., 1981. Volcanic-associated massive sulphide deposits. In: Skinner, B.J. (Ed.), Economic Geology 75th Anniversary Volume. Society of Economic Geologists, Boulder, Colorado, pp. 485–627.

Franklin, J.M., Gibson, H.L., Jonasson, I.R., Galley, A.G., 2005. Volcanogenic massive sulfide deposits. In: Hedenquist, J.W., Thompson, J.F.H., Goldfarb, R.J., Richards, J.P. (Eds.), Economic Geology 100th Anniversary Volume. Society of Economic Geologists, Boulder, Colorado, pp. 523–560.

Galley, A.G., Hannington, M.D., Jonasson, I.R., 2007. Volcanogenic massive sulphide deposits. In: Goodfellow, W.D. (Ed.), Mineral Deposits of Canada: A Synthesis of Major Deposit Types: Geological Association of Canada, Mineral Deposits Division and Geological Survey of Canada Special Publication, 5, pp. 141–162.

Geringer, G.J., Botha, B.J.V., Pretorius, J.J., Ludick, D.J., 1986. Calc-alkaline volcanism along the eastern margin of the Namaqua Mobile Belt, South Africa – a possible middle Proterozoic volcanic arc. Precambrian Research 33, 139–170.

Geringer, G.J., Botha, B.J.V., Slabbert, M.J., 1988. The Keimoes Suite – a composite granitoid batholith along the eastern margin of the Namaqua mobile belt, South Africa. South African Journal of Geology 91, 465–476.

Geringer, G.J., Humphreys, H.C., Scheepers, D.J., 1994. Lithostratigraphy, protolithology, and tectonic setting of the Areachap Group along the eastern margin of the Namaqua Mobile Belt, South Africa. South African Journal of Geology 97, 78–100.

Ghavami-Riabi, R., 2006. Geochemical exploration for base metal sulphide deposits in an arid environment (eastern Namaqua Metamorphic Province), South Africa. Unpublished Ph.D. Thesis, University of Pretoria, Pretoria, 181 pp.

Gifkins, C.C., Herrmann, W., Large, R., 2005. Altered volcanic rocks: A guide to description and interpretation. Centre for Ore Deposit Research (CODES) Special Publication. University of Tasmania, Hobart, Tasmania, Australia. 275 pp.

Gorton, R.K., 1981. The petrology of the Kielder sulfide deposits and their wall rocks: District of Prieska, N. Cape, South Africa. Unpublished M.Sc. dissertation, University of Cape Town, 153 pp.

Humphreys, H.C., Van Bever Donker, J.M., Scott, W.D., Van Schalkwyk, L., 1988. The early deformational history of the eastern Namaqua Province: new evidence from Prieska Copper Mines. South African Journal of Geology 91, 174–183.

Ishikawa, Y., Sawaguchi, T., Iwaya, S., Horiuchi, M., 1976. Delineation of prospecting targets for Kuroko deposits based on modes of volcanism of underlying dacite and alteration halos. Mining Geology 26, 105–117.

Köppel, V., 1980. Lead-isotope studies of stratiform ore deposits of Namaqualand, N.W. Cape province, South Africa, and their implications on the age of the Bushmanland sequence. In: Ridge, J.D. (Ed.), 5th IAGOD Symposium, Schweizerbart'sche, Stuttgart, pp. 195–207.

Large, R.R., Gemmell, J.B., Paulick, H., Huston, D.L., 2001. The alteration box plot: A simple approach to understanding the relationship between alteration mineralogy and lithogeochemistry associated with volcanic-hosted massive sulfide deposits. Economic Geology 96, 957–972.

Ludwig, K.R., 2003. Isoplot / Ex (version 3.00). A geochronological toolkit for Microsoft Excel. Berkeley Geochronology Center. Special Publication 4, 1–71.

McDonough, W.F., Sun, S., Ringwood, A.E., Jagoutz, E., Hofmann, A.W., 1991. K, Rb and Cs in the earth and moon and the evolution of the earth's mantle. Geochimica et Cosmochimica Acta 56, 1001–1012.

Middleton, R.C., 1976. The geology of the Prieska Copper Mines (Pty.) Ltd. Economic Geology 71, 328–350.

Moen, H.F.G., 2007. The geology of the Upington area. Explanation, map sheet 2820 (Scale: 1:250 000), Council for Geoscience, Pretoria, 160 pp.

Nakamura, N., 1974. Determination of REE, Ba, Fe, Mg, Na and K in carbonaceous and ordinary chondrites. Geochemica et Cosmochimica Acta 38, 757–775.

Norrish, K., Hutton, J.T., 1969. An accurate X-ray fluorescence spectrographic method for the analysis of a wide range of geological samples. Geochimica et Cosmochimica Acta 33, 431–453.

Pearce, J.A., Norry, M.J., 1979. Petrogenetic implications of Ti, Zr, Y and Nb variations in volcanic rocks. Contributions to Mineralogy and Petrology 69, 33–47.

Pearce, J.A., Harris, N.B.W., Tindle, A.G., 1984. Trace element discrimination diagrams for the tectonic discrimination of granitic rocks. Journal of Petrology 25, 956–983.

Pettersson, A., Cornell, D.H., Moen, H.F.G., Reddy, S., Evans, D., 2007. Ion-probe dating of 1.2 Ga collision and crustal architecture in the Namaqua-Natal Province of southern Africa. Precambrian Research 158, 79–92.

Robertson, S., 1999. BGS Rock Classification Scheme, volume 2: Classification of metamorphic rocks. British Geological Survey Research Report, RR 99–02. 26 pp.

Schade, J., Cornell, D.H., Theart, H.F.J., 1989. Rare earth element and isotopic evidence for the genesis of the Prieska massive sulfide deposit, South Africa. Economic Geology 84, 49–63.

Scheepers, D.J., 1989. The petrology and geochemistry of the Vogelstruisbult Annex Cu-Zn deposit in the Prieska district, north-western Cape Province. Unpublished M.Sc. Thesis, University of Stellenbosch, 131 pp.

Solomon, M., Tornos, F., Large, R.R., Badham, J.N.P., Both, R.A., Zaw, Khin, 2004. Zn-Pb-Cu volcanic-hosted massive sulphide deposits: criteria for distinguishing brine pool-type from black smoker-type sulphide deposition. Ore Geology Reviews 25, 269–283.

Stüeken, E.E., 2006. Volcanogenic massive sulphide deposits of the Areachap Group. Internship Project, University of Johannesburg, South Africa. 39 pp.

Theart, H.F.J., 1985. Copperton-Areachap Cu, Zn mineralisation. Unpublished Ph.D. thesis, University of Stellenbosch, 329 pp.

Theart, H.F.J., Cornell, D.H., Schade, J., 1989. Geochemistry and metamorphism of the Prieska Zn-Cu deposit, South Africa. Economic Geology 84, 34–49.

Theart, H.F.J., Ghavami-Riabi, R., Mouri, H., Gräser, P., in press. Applying the box plot to the recognition of footwall alteration zones related to VMS deposits in a high-grade metamorphic terrain, South Africa, a lithogeochemical exploration application. Chemie der Erde – Geochemistry. doi:10.1016/j.chemer.2010.09.002.

Thomas, R.J., Cornell, D.H., Moore, J.M., Jacobs, J., 1994. Crustal evolution of the Namaqua-Natal Metamorphic province, southern Africa. South African Journal of Geology 97, 8–14.

Uiterwyk, B.H., Frick, C., 1985. The mineralogy, petrology and geochemistry of the Prieska ore-body, Copperton, N.W. Cape Province. Bulletin of the Geological Survey of South Africa 78. 38 pp.

Verati, C., Lancelot, J., Hékinian, R., 1999. Pb isotope study of black smokers and basalts from Pito Seamount site (Easter microplate). Chemical Geology 155, 45–63.

Voet, H.W., King, B.H., 1986. The Areachap copper-zinc deposit, Gordonia district. In: Anhaeusser, C.R., Maske, S. (Eds.), Mineral deposits of southern Africa, II. Geological Society of South Africa, Johannesburg, pp. 1529–1537.

Vokes, F.M., 2000. Ores and metamorphism: Introduction and historical perspective. Reviews in Economic Geology 11, 148–160.

Wagener, J.H.F., Van Schalkwyk, L., 1986. The Prieska zinc-copper deposit, north-western Cape Province. In: Anhaeusser, C.R., Maske, S. (Eds.), Mineral deposits of southern Africa, II. Geological Society of South Africa, Johannesburg, pp. 1503–1527.

Williams, I.S., 1998. U-Th-Pb geochronology by ion microprobe. In: McKibben, M.A., Shanks, W.C., Ridley, W.I. (Eds.), Applications of microanalytical techniques to understanding mineralising processes: Reviews in Economic Geology, 7, pp. 1–35.

Winchester, J.A., Floyd, P.A., 1977. Geochemical discrimination of different magma series and their differentiation products using immobile elements. Chemical Geology 20, 325–343.

Wood, D.A., 1980. The application of a Th-Hf-Ta diagram to problems of tectonomagmatic classification and to establishing the nature of crustal contamination of basaltic lavas of the British Tertiary volcanic province. Earth and Planetary Science Letters 50, 11–30.